Published OnlineFirst September 7, 2012; DOI: 10.1158/1940-6207.CAPR-12-0056

its evaluation based on serum pepsinogen tests is a useful means of assessing cancer risk (12, 20). To evaluate the relationship between *RASGRF1* methylation and mucosal atrophy, we divided the samples based on the pepsinogen test results and then generated respective ROC curves. Notably, *RASGRF1* methylation was highly discriminative between healthy individuals and patients with gastric cancer irrespective of the pepsinogen test results (Fig. 3C and Table 2), which suggests that the strong association between *RASGRF1* methylation and gastric cancer is independent of gastric mucosal atrophy. This could make *RASGRF1* methylation a powerful biomarker with which to identify individuals at high risk for gastric cancer.

Functional analysis of *RASGRF1* in gastric cancer cells

Finally, we tested whether *RASGRF1* serves as a tumor suppressor in gastric cancer. Gastric cancer cell lines were transfected with a *RASGRF1* expression vector or a negative control, after which colony formation assays were carried out with the transfectants. Western blot analysis confirmed that the transfectants expressed exogenous RASGRF1 (Supplementary Fig. S4). Moreover, introduction of *RASGRF1* markedly suppressed colony formation by the cell lines tested (Fig. 4A and B). When we then carried out Matrigel invasion assays to test the effect of *RASGRF1* expression on gastric cancer cell invasion; we observed marked inhibition of cell invasion by SNU638 cells expressing *RASGRF1* (Fig. 4C). These results suggest that *RASGRF1* may play a tumor suppressor role that is itself suppressed in gastric cancer.

Discussion

Identification of individuals at high risk of developing gastric cancer is essential for the prevention and early detection of gastric cancer. Esophagogastroduodenoscopy (EGD) is the most useful method for detecting gastric cancers, although population-based screening for gastric cancers using only EGD is generally considered ineffective for reducing mortality (21, 22). Severe atrophic gastritis is strongly associated with an increased risk of intestinal gastric cancer, and screening for high-risk individuals based on serum pepsinogen levels followed by careful observation using EGD is an effective strategy for surveillance of this disease (12, 23). In contrast, diffuse type gastric cancers lack those characteristic features because they do not progress through atrophic gastritis. Consequently, identification of sensitive and reliable biomarkers for diffuse type gastric cancer would be highly desirable. A number of studies have shown aberrant DNA methylation in precancerous lesions, including chronic gastritis and intestinal metaplasia, and detection of such an epigenetic field defect would provide useful information for identifying individuals at high risk for developing gastric cancer (7, 24, 25). The majority of those studies focused on well-studied genes, such as *CDH1* and *p16* (26, 27), but recent advances in microarray technology have enabled us to conduct a genome-wide analysis of CpG island methylation status. For instance, a recent study reported by Nanjo and colleagues identified a series of 7 methylation markers that can predict gastric cancer risk in individuals with past *H. pylori* infection (28).

In this study, we carried out high-throughput methylation analysis using a set of gastric mucosa specimens from healthy individuals and patients with intestinal or diffuse type gastric cancer. Our MCAM analysis identified a number of methylated genes in noncancerous gastric mucosae from the patients with gastric cancer. A larger number of methylated genes were identified in gastric mucosae from patients with intestinal type gastric cancer than with diffuse type gastric cancer, which is consistent with the earlier observation that aberrant DNA methylation is not induced by the presence of *H. pylori*, itself, but by inflammatory processes triggered by the infection (29). Our list of genes methylated in the background mucosa in intestinal type gastric cancer includes a number of methylation-prone genes (e.g., *SFRP2* and *IRF4*) that confirms the reliability of our screening method (13, 30). The methylation status in

Table 2. ROC analysis of the ability of *RASGRF1* methylation to discriminate between patients with gastric cancer and healthy individuals

	AUC			Sensitivity		Specificity	
	Estimate	95% confidence interval (CI)	Cut-off	Estimate	95% CI	Estimate	95% CI
Total (n = 161)	0.821	(0.775%–0.887%)	7.71%	78.02%	(68.12%–86.03%)	75.36%	(63.51%–84.94%)
			11.68%	74.73%	(64.53%–83.25%)	84.06%	(73.26%–91.76%)
			12.76%	70.33%	(59.84%–79.45%)	86.96%	(86.68%–93.86%)
PG-positive (n = 35)	0.763	(0.601%–0.926%)	6.79%	80.00%	(56.34%–94.27%)	60.00%	(32.29%–83.66%)
			13.67%	70.00%	(45.72%–88.11%)	86.67%	(59.54%–98.34%)
			22.29%	55.00%	(31.53%–76.94%)	93.33%	(68.05%–99.83%)
PG-negative (n = 41)	0.844	(0.719%–0.969%)	7.13%	77.78%	(52.36%–93.59%)	73.91%	(51.60%–89.77%)
			10.64%	72.22%	(46.52%–90.31%)	86.96%	(66.41%–97.22%)
			13.39%	6.67%	(40.99%–86.66%)	91.30%	(71.96%–98.93%)

Published OnlineFirst September 7, 2012; DOI: 10.1158/1940-6207.CAPR-12-0056

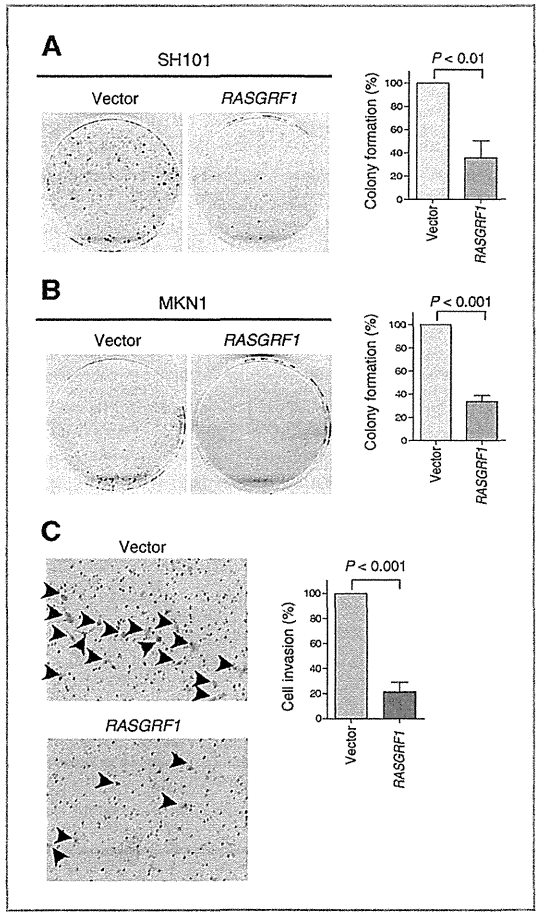

Figure 4. Functional analysis of *RASGRF1*. A and B, colony formation assays using the indicated gastric cancer cells transfected with a *RASGRF1* expression vector or a control vector. Representative results are on the left, and relative colony formation efficiencies are on the right. Shown are means of 3 replications; error bars represent SDs. C, Matrigel invasion assay using SNU638 cells transfected with a *RASGRF1* expression vector or a control vector. Invading cells are indicated by arrows. Shown on the right are the means of 3 random microscopic fields per membrane; error bars represent the SDs.

the background mucosa of diffuse type gastric cancer had remained largely unknown and, to our knowledge, this study is the first to examine the genome-wide CpG island methylation status in the gastric mucosa from diffuse type patients with gastric cancer. It is noteworthy that we found that approximately half of the genes methylated in diffuse type gastric cancer were also methylated in intestinal type gastric cancer. It is generally believed that intestinal and diffuse type gastric cancers develop through distinctly different molecular pathways; however, our data may be indicative of a pathogenic mechanism common to both types. Furthermore, our results suggest that methylation of these genes could be an ideal molecular marker for assessing the risk for both gastric cancer types.

Among the genes identified, we selected *RASGRF1*, *GALNT14*, and *SOX5* for further analysis and found that the elevation of their methylation levels was specific to patients with gastric cancer. *SOX5* is a member of the high-mobility group superfamily and is reportedly overexpressed in several malignancies, including nasopharyngeal carcinoma and prostate cancer, which suggests it has oncogenic properties (31, 32). On the other hand, one recent study showed that *SOX5* suppresses platelet-derived growth factor B–induced gliomas (33). *GALNT14* belongs to a large subfamily of glycosyltransferases, and its expression in cancer cells is associated with cellular sensitivity to the proapoptotic ligand Apo2L/TRAIL (34). Up to now, however, methylation of *GALNT14* and *SOX5* has not been reported in human cancer, and further study will be needed to clarify their functional significance.

RASGRF1 and *RASGRF2* constitute a gene family encoding guanine nucleotide exchange factors (GEF), which activate Ras GTPase by promoting the release of bound GDP, enabling activating GTP to take its place (35). RASGRF proteins are predominantly expressed in adult neurons in the central nervous system, and are involved in a wide range of neuronal functions. In mice, *Rasgrf1* is an imprinted gene. The imprinted *Rasgrf1* locus is methylated on the paternal allele at a differentially methylated region (DMR) located 30 kb upstream of the promoter, and it is expressed only from the paternal allele (36). Interestingly, a recent study showed that Piwi-interacting RNAs (piRNAs), a subset of noncoding small RNAs, play a pivotal role in the establishment of methylation at the *Rasgrf1* DMR (37). In contrast, we found the promoter CpG island of *RASGRF1* to be hypermethylated in gastric cancer, and that this methylation is unlikely to be associated with gene imprinting. Levels of *RASGRF1* methylation are also significantly elevated in the noncancerous background gastric mucosa in both the intestinal and diffuse types of gastric cancer and are highly discriminative between gastric mucosa from cancer-free individuals and patients with gastric cancer. This suggests *RASGRF1* methylation may be a gastric cancer risk factor that is independent of gastric mucosal atrophy, and that *RASGRF1* methylation could be a predictive marker of gastric cancer risk that would overcome the disadvantages of other screening methods, such as the serum pepsinogen test and EGD.

The function of *RASGRF1* in normal stomach and during gastric tumorigenesis is largely unknown, but it may exert oncogenic effects through activation of Ras proteins (35). On the other hand, one recent study showed that RASGRF proteins bind directly to Cdc42, another Ras-related GTP-binding protein, and suppress Cdc42-mediated cellular processes, including tumor cell invasion and transformation (38). In this study, we found that ectopic expression of *RASGRF1* suppressed proliferation and invasion by gastric cancer cells, which is suggestive of its tumor suppressor role, although we carried out only overexpression experiments. Alteration of *RASGRF1* gene in human cancer has not yet been reported; in fact, this is the first report of its epigenetic

Published OnlineFirst September 7, 2012; DOI: 10.1158/1940-6207.CAPR-12-0056

silencing, and further study will be needed to clarify its function in carcinogenesis.

In summary, we have comprehensively analyzed the DNA methylation status of gastric mucosa specimens from patients with gastric cancer. We identified a number of methylated genes that might be involved in an epigenetic field defect in the stomach. Among them, *RASGRF1* is a novel gastric cancer–associated gene prevalently methylated in the background mucosa in both intestinal and diffuse type gastric cancer. The combination of a DNA methylation test using *RASGRF1* as a marker with a pepsinogen test or EGD would greatly improve the efficacy of risk assessment and surveillance of gastric cancers.

Disclosure of Potential Conflicts of Interest

No potential conflicts of interest were disclosed.

Authors' Contributions

Conception and design: E. Yamamoto, H. Suzuki, T. Sugai, K. Imai, M. Toyota, Y. Shinomura
Development of methodology: E. Yamamoto, H. Yamano
Acquisition of data (provided animals, acquired and managed patients, provided facilities, etc.): H. Takamaru, E. Yamamoto, H. Yamano, K. Yoshikawa, T. Harada, R. Suzuki, H. Yamamoto, M. Kai, T. Sugai
Analysis and interpretation of data (e.g., statistical analysis, biostatistics, computational analysis): H. Takamaru, E. Yamamoto, M. Nojima, R. Maruyama, T. Sugai
Writing, review, and/or revision of the manuscript: H. Takamaru, E. Yamamoto, H. Suzuki, T. Sugai
Administrative, technical, or material support (i.e., reporting or organizing data, constructing databases): E. Yamamoto, H. Yamano, T. Kimura, M. Ashida, R. Suzuki, H. Yamamoto, T. Sugai
Study supervision: H. Suzuki, T. Tokino, K. Imai, M. Toyota, Y. Shinomura

Acknowledgments

The authors thank Dr. Yutaka Kondo for technical assistance with the MCAM and Dr. William F. Goldman for editing the manuscript.

Grant Support

This study was supported in part by a Grants-in-Aid for Scientific Research (B) from the Japan Society for Promotion of Science (to Y. Shinomura), a Grant-in-Aid for the Third-term Comprehensive 10-year Strategy for Cancer Control (to M. Toyota and H. Suzuki), a Grant-in-Aid for Cancer Research from the Ministry of Health, Labor, and Welfare, Japan (to M. Toyota and H. Suzuki), A3 foresight program from the Japan Society for Promotion of Science (to H. Suzuki), and the Takeda Science Foundation (to E. Yamamoto).

The costs of publication of this article were defrayed in part by the payment of page charges. This article must therefore be hereby marked *advertisement* in accordance with 18 U.S.C. Section 1734 solely to indicate this fact.

Received February 6, 2012; revised July 8, 2012; accepted August 14, 2012; published OnlineFirst September 7, 2012.

References

1. Uemura N, Okamoto S, Yamamoto S, Matsumura N, Yamaguchi S, Yamakido M, et al. *Helicobacter pylori* infection and the development of gastric cancer. N Engl J Med 2001;345:784–9.
2. Yuasa Y. Control of gut differentiation and intestinal-type gastric carcinogenesis. Nat Rev Cancer 2003;3:592–600.
3. Yamamoto E, Suzuki H, Takamaru H, Yamamoto H, Toyota M, Shinomura Y. Role of DNA methylation in the development of diffuse-type gastric gancer. Digestion 2011;83:241–9.
4. Jones PA, Baylin SB. The fundamental role of epigenetic events in cancer. Nat Rev Genet 2002;3:415–28.
5. Suzuki H, Tokino T, Shinomura Y, Imai K, Toyota M. DNA methylation and cancer pathways in gastrointestinal tumors. Pharmacogenomics 2008;9:1917–28.
6. Chan AO, Lam SK, Wong BC, Wong WM, Yuen MF, Yeung YH, et al. Promoter methylation of E-cadherin gene in gastric mucosa associated with *Helicobacter pylori* infection and in gastric cancer. Gut 2003;52:502–6.
7. Maekita T, Nakazawa K, Mihara M, Nakajima T, Yanaoka K, Iguchi M, et al. High levels of aberrant DNA methylation in *Helicobacter pylori*-infected gastric mucosae and its possible association with gastric cancer risk. Clin Cancer Res 2006;12:989–95.
8. Yamamoto E, Toyota M, Suzuki H, Kondo Y, Sanomura T, Murayama Y, et al. LINE-1 hypomethylation is associated with increased CpG island methylation in *Helicobacter pylori*-related enlarged-fold gastritis. Cancer Epidemiol Biomarkers Prev 2008;17:2555–64.
9. Suzuki H, Yamamoto E, Nojima M, Kai M, Yamano HO, Yoshikawa K, et al. Methylation-associated silencing of microRNA-34b/c in gastric cancer and its involvement in an epigenetic field defect. Carcinogenesis 2010;31:2066–73.
10. Ando T, Yoshida T, Enomoto S, Asada K, Tatematsu M, Ichinose M, et al. DNA methylation of microRNA genes in gastric mucosae of gastric cancer patients: its possible involvement in the formation of epigenetic field defect. Int J Cancer 2009;124:2367–74.
11. Dixon MF, Genta RM, Yardley JH, Correa P. Classification and grading of gastritis. The updated Sydney System. International Workshop on the Histopathology of Gastritis, Houston 1994. Am J Surg Pathol 1996;20:1161–81.
12. Miki K, Morita M, Sasajima M, Hoshina R, Kanda E, Urita Y. Usefulness of gastric cancer screening using the serum pepsinogen test method. Am J Gastroenterol 2003;98:735–9.
13. Nojima M, Suzuki H, Toyota M, Watanabe Y, Maruyama R, Sasaki S, et al. Frequent epigenetic inactivation of SFRP genes and constitutive activation of Wnt signaling in gastric cancer. Oncogene 2007;26:4699–713.
14. Yanagihara K, Ito A, Toge T, Numoto M. Antiproliferative effects of isoflavones on human cancer cell lines established from the gastrointestinal tract. Cancer Res 1993;53:5815–21.
15. Yanagihara K, Tsumuraya M. Transforming growth factor beta 1 induces apoptotic cell death in cultured human gastric carcinoma cells. Cancer Res 1992;52:4042–5.
16. Toyota M, Ho C, Ahuja N, Jair KW, Li Q, Ohe-Toyota M, et al. Identification of differentially methylated sequences in colorectal cancer by methylated CpG island amplification. Cancer Res 1999;59:2307–12.
17. Gao W, Kondo Y, Shen L, Shimizu Y, Sano T, Yamao K, et al. Variable DNA methylation patterns associated with progression of disease in hepatocellular carcinomas. Carcinogenesis 2008;29:1901–10.
18. Goto Y, Shinjo K, Kondo Y, Shen L, Toyota M, Suzuki H, et al. Epigenetic profiles distinguish malignant pleural mesothelioma from lung adenocarcinoma. Cancer Res 2009;69:9073–82.
19. Suzuki H, Takatsuka S, Akashi H, Yamamoto E, Nojima M, Maruyama R, et al. Genome-wide profiling of chromatin signatures reveals epigenetic regulation of MicroRNA genes in colorectal cancer. Cancer Res 2011;71:5646–58.
20. Yanaoka K, Oka M, Mukoubayashi C, Yoshimura N, Enomoto S, Iguchi M, et al. Cancer high-risk subjects identified by serum pepsinogen tests: outcomes after 10-year follow-up in asymptomatic middle-aged males. Cancer Epidemiol Biomarkers Prev 2008;17:838–45.
21. Inaba S, Hirayama H, Nagata C, Kurisu Y, Takatsuka N, Kawakami N, et al. Evaluation of a screening program on reduction of gastric cancer mortality in Japan: preliminary results from a cohort study. Prev Med 1999;29:102–6.
22. Riecken B, Pfeiffer R, Ma JL, Jin ML, Li JY, Liu WD, et al. No impact of repeated endoscopic screens on gastric cancer mortality in a

Published OnlineFirst September 7, 2012; DOI: 10.1158/1940-6207.CAPR-12-0056

prospectively followed Chinese population at high risk. Prev Med 2002;34:22–8.
23. Melton SD, Genta RM, Souza RF. Biomarkers and molecular diagnosis of gastrointestinal and pancreatic neoplasms. Nat Rev Gastroenterol Hepatol 2010;7:620–8.
24. Kang GH, Lee HJ, Hwang KS, Lee S, Kim JH, Kim JS. Aberrant CpG island hypermethylation of chronic gastritis, in relation to aging, gender, intestinal metaplasia, and chronic inflammation. Am J Pathol 2003;163:1551–6.
25. Nakajima T, Maekita T, Oda I, Gotoda T, Yamamoto S, Umemura S, et al. Higher methylation levels in gastric mucosae significantly correlate with higher risk of gastric cancers. Cancer Epidemiol Biomarkers Prev 2006;15:2317–21.
26. Leung WK, Man EP, Yu J, Go MY, To KF, Yamaoka Y, et al. Effects of *Helicobacter pylori* eradication on methylation status of E-cadherin gene in noncancerous stomach. Clin Cancer Res 2006;12:3216–21.
27. Dong CX, Deng DJ, Pan KF, Zhang L, Zhang Y, Zhou J, et al. Promoter methylation of p16 associated with *Helicobacter pylori* infection in precancerous gastric lesions: a population-based study. Int J Cancer 2009;124:434–9.
28. Nanjo S, Asada K, Yamashita S, Nakajima T, Nakazawa K, Maekita T, et al. Identification of gastric cancer risk markers that are informative in individuals with past *H. pylori* infection. Gastric Cancer. 2012 Jan 12. [Epub ahead of print].
29. Niwa T, Tsukamoto T, Toyoda T, Mori A, Tanaka H, Maekita T, et al. Inflammatory processes triggered by *Helicobacter pylori* infection cause aberrant DNA methylation in gastric epithelial cells. Cancer Res 2010;70:1430–40.
30. Yamashita M, Toyota M, Suzuki H, Nojima M, Yamamoto E, Kamimae S, et al. DNA methylation of interferon regulatory factors in gastric cancer and noncancerous gastric mucosae. Cancer Sci 2010;101:1708–16.
31. Huang DY, Lin YT, Jan PS, Hwang YC, Liang ST, Peng Y, et al. Transcription factor SOX-5 enhances nasopharyngeal carcinoma progression by down-regulating SPARC gene expression. J Pathol 2008;214:445–55.
32. Ma S, Chan YP, Woolcock B, Hu L, Wong KY, Ling MT, et al. DNA fingerprinting tags novel altered chromosomal regions and identifies the involvement of SOX5 in the progression of prostate cancer. Int J Cancer 2009;124:2323–32.
33. Tchougounova E, Jiang Y, Brasater D, Lindberg N, Kastemar M, Asplund A, et al. Sox5 can suppress platelet-derived growth factor B-induced glioma development in Ink4a-deficient mice through induction of acute cellular senescence. Oncogene 2009;28:1537–48.
34. Wagner KW, Punnoose EA, Januario T, Lawrence DA, Pitti RM, Lancaster K, et al. Death-receptor O-glycosylation controls tumor-cell sensitivity to the proapoptotic ligand Apo2L/TRAIL. Nat Med 2007;13:1070–7.
35. Feig LA. Regulation of neuronal function by Ras-GRF exchange factors. Genes Cancer 2011;2:306–19.
36. Yoon BJ, Herman H, Sikora A, Smith LT, Plass C, Soloway PD. Regulation of DNA methylation of Rasgrf1. Nat Genet 2002;30:92–6.
37. Watanabe T, Tomizawa S, Mitsuya K, Totoki Y, Yamamoto Y, Kuramochi-Miyagawa S, et al. Role for piRNAs and noncoding RNA in *de novo* DNA methylation of the imprinted mouse Rasgrf1 locus. Science 2011;332:848–52.
38. Calvo F, Sanz-Moreno V, Agudo-Ibanez L, Wallberg F, Sahai E, Marshall CJ, et al. RasGRF suppresses Cdc42-mediated tumour cell movement, cytoskeletal dynamics and transformation. Nat Cell Biol 2011;13:819–26.

Published OnlineFirst January 18, 2012; DOI: 10.1158/0008-5472.CAN-11-1803

Molecular and Cellular Pathobiology

Cancer Research

Upregulation of miR-196a and *HOTAIR* Drive Malignant Character in Gastrointestinal Stromal Tumors

Takeshi Niinuma[1], Hiromu Suzuki[1,3], Masanori Nojima[4], Katsuhiko Nosho[1], Hiroyuki Yamamoto[1], Hiroyuki Takamaru[1], Eiichiro Yamamoto[3], Reo Maruyama[3], Takayuki Nobuoka[2], Yasuaki Miyazaki[9], Toshirou Nishida[9,10], Takeo Bamba[11], Tatsuo Kanda[11], Yoichi Ajioka[12], Takahiro Taguchi[13], Satoshi Okahara[7], Hiroaki Takahashi[7], Yasunori Nishida[8], Masao Hosokawa[8], Tadashi Hasegawa[5], Takashi Tokino[6], Koichi Hirata[2], Kohzoh Imai[14], Minoru Toyota[3], and Yasuhisa Shinomura[1]

Abstract

Large intergenic noncoding RNAs (lincRNA) have been less studied than miRNAs in cancer, although both offer considerable theranostic potential. In this study, we identified frequent upregulation of miR-196a and lincRNA *HOTAIR* in high-risk gastrointestinal stromal tumors (GIST). Overexpression of miR-196a was associated with high-risk grade, metastasis and poor survival among GIST specimens. miR-196a genes are located within the *HOX* gene clusters and microarray expression analysis revealed that the *HOXC* and *HOTAIR* gene were also coordinately upregulated in GISTs which overexpress miR-196a. In like manner, overexpression of *HOTAIR* was also strongly associated with high-risk grade and metastasis among GIST specimens. RNA interference–mediated knockdown of *HOTAIR* altered the expression of reported *HOTAIR* target genes and suppressed GIST cell invasiveness. These findings reveal concurrent overexpression of *HOX* genes with noncoding RNAs in human cancer in this setting, revealing miR-196a and *HOTAIR* as potentially useful biomarkers and therapeutic targets in malignant GISTs. *Cancer Res; 72(5); 1126–36. ©2012 AACR.*

Introduction

Gastrointestinal stromal tumors (GIST) are the most common mesenchymal tumors of the gastrointestinal tract (1–3). GISTs arise predominantly in the stomach (60%) and small intestine (25%) but also occur in colon and rectum (5%), esophagus (2%), and other organs (3). Immunohistochemically, GISTs are positive for KIT and CD34 and are negative or variably positive for other neural and smooth muscle cell markers. The expression of KIT and CD34 is a characteristic feature of the intestinal cells of Cajal (ICC), which are located in the intestinal wall and regulate gastrointestinal motility. GISTs are thus thought to originate from ICCs or ICC precursors. Activating *KIT* mutations have been identified in 80% to 90% of GISTs, and mutation of the platelet-derived growth factor receptor alpha gene (*PDGFRA*) is observed in approximately 5% of GISTs (1–3). In that context, imatinib mesylate (formerly STI571) was developed as a tyrosine kinase inhibitor and has been shown to inhibit the activities of BCR-ABL, KIT, and PDGFR. Imatinib mesylate is currently being used for the treatment of both chronic myeloid leukemia and metastatic GISTs.

Predicting the biologic potential of GISTs is often difficult, and considerable effort has been made to define the variables that could enable more accurate identification of tumors with malignant potential. In most classification systems, the key prognostic factors for estimating malignant potential are tumor size and mitotic rate, and to a more variable degree, the proliferation index or tumor site (4). Other potential and promising markers of GIST malignancy are molecular alterations. As mentioned, a large majority of GISTs exhibit activating *KIT* or *PDGFRA* mutations. By itself, however, mutation status does not fully explain the diverse biology of GISTs, and it is believed that additional molecular alterations are required for the progression of high-risk GISTs. For instance, expression of CD26 (encoded by *DPP4*) is strongly associated with poor survival among patients with gastric GISTs, suggesting its involvement in the malignant progression of the disease (5).

Authors' Affiliations: First Departments of [1]Internal Medicine and [2]Surgery, Departments of [3]Molecular Biology, [4]Public Health, [5]Surgical Pathology, [6]Medical Genome Science, Research Institute for Frontier Medicine, Sapporo Medical University School of Medicine; Departments of [7]Gastroenterology and [8]Surgery, Keiyukai Sapporo Hospital, Sapporo; [9]Department of Surgery, Osaka University Graduate School of Medicine; [10]Department of Surgery, Osaka Police Hospital, Osaka; Divisions of [11]Digestive and General Surgery and [12]Molecular and Diagnostic Pathology, Niigata University Graduate School of Medical and Dental Sciences, Niigata; [13]Division of Human Health and Medical Science, Graduate School of Kuroshio Science, Kochi University, Nankoku; and [14]Division of Novel Therapy for Cancer, The Advanced Clinical Research Center, The Institute of Medical Science, The University of Tokyo, Tokyo, Japan

Note: Supplementary data for this article are available at Cancer Research Online (http://cancerres.aacrjournals.org/).

T. Niinuma and H. Suzuki contributed equally to this work.

Corresponding Authors: Hiromu Suzuki, Department of Molecular Biology, Sapporo Medical University; S1, W17, Chuo-Ku, Sapporo 060-8556, Japan. Phone: 81-11-611-2111; Fax: 81-11-622-1918; *E-mail: hsuzuki@sapmed.ac.jp; and Yasuhisa Shinomura*, First Department of Internal Medicine, Sapporo Medical University; S1, W16, Chuo-Ku, Sapporo 060-8543, Japan. Fax: 81-11-611-2282; E-mail: shinomura@sapmed.ac.jp

doi: 10.1158/0008-5472.CAN-11-1803

Published OnlineFirst January 18, 2012; DOI: 10.1158/0008-5472.CAN-11-1803

In addition, we recently showed that hypomethylation of repetitive DNA elements is predominantly observed in malignant GISTs, and that global hypomethylation correlates with increased chromosomal aberration (6).

miRNAs are a class of small noncoding RNAs that regulate gene expression by inducing translational inhibition or direct degradation of target mRNAs through base pairing to partially complementary sites (7). miRNAs are highly conserved among species and play critical roles in a variety of biologic processes, including development, differentiation, cell proliferation, and apoptosis. Consistent with their role in these processes, a number of studies have shown widespread alteration of miRNA expression patterns in cancer (8, 9). It has also been shown that in cancer global miRNA expression profiles, as well as expression of specific miRNAs, correlate with disease prognosis and clinical outcome (10). To date, however, only a few groups have studied miRNA expression in GISTs (11, 12), and no specific miRNAs that could serve as prognostic markers have yet been identified.

In this study, we investigated the global pattern of miRNA expression in GISTs. Our aim was to evaluate the contribution made by miRNAs to the malignant potential of GISTs and to identify predictive biomarkers. We determined that upregulation of miR-196a is strongly associated with high risk and poor prognosis in GIST patients. Furthermore, we provide evidence that overexpression of miR-196a is accompanied by upregulation of *HOXC* cluster genes and a metastasis-associated noncoding RNA in GISTs.

Materials and Methods

Tumor samples

A total of 56 fresh frozen GIST specimens were obtained from Sapporo Medical University Hospital, Keiyukai Sapporo Hospital, and Osaka University Hospital, as described (6). In addition, formalin-fixed paraffin-embedded (FFPE) tissue sections of 100 GIST specimens were obtained from Niigata University Hospital. Informed consent was obtained from all patients before collection of the specimens, and this study was approved by the respective Institutional Review Boards. Risk grade was assessed according to the risk definition system proposed by Fletcher and colleagues (4). Tumors that were less than 2 cm in diameter with a mitotic count of less than 5/50 high-power fields (HPF) were categorized as very low risk. Tumors that were 2 to 5 cm in diameter with a mitotic count of less than 5/50 HPF were considered to be low risk. Tumors that were less than 5 cm in diameter with a mitotic count of 6 to 10/50 HPF, or were 5 to 10 cm with a mitotic count of less than 5/50 HPF were considered to be intermediate risk. Tumors that were more than 5 cm in diameter with a mitotic count of more than 5/50 HPF, more than 10 cm in diameter with any mitotic count, or any size with a mitotic count of more than 10/50 HPF were considered to be high risk. Total RNA was extracted from fresh frozen tissue specimens using a mirVana miRNA Isolation Kit (Ambion). Total RNA was extracted from FFPE tissue specimens using a RecoverAll Total Nucleic Acid Isolation Kit for FFPE (Ambion). Tumor tissues were reviewed by pathologists and were macrodissected; laser capture microdissection was not carried out in this study.

miRNA microarray analysis

One-color microarray-based miRNA expression analysis was carried out according to the manufacturer's instructions (Agilent Technologies). Briefly, 100 ng of total RNA from fresh frozen GIST tissues was labeled using miRNA Labeling Reagent (Agilent Technologies), after which the labeled RNA was hybridized to a Human miRNA Microarray V3 (Rel 12.0, G4470C; Agilent Technologies), which covers 859 human miRNAs and 80 viral miRNAs. The microarray data were analyzed using GeneSpring GX version 11 (Agilent Technologies). The normalized microarray data were then compared with the TaqMan assay results using GraphPad PRISM version 5 (GraphPad Software Inc.). The Gene Expression Omnibus accession number for the miRNA microarray data is GSE31741.

Quantitative RT-PCR of miRNA

miR-196a expression was analyzed using TaqMan microRNA Assays (Applied Biosystems). Briefly, 5 ng of total RNA were reverse transcribed using specific stem-loop RT primers, after which they were amplified and detected using PCR with specific primers and TaqMan probes. The PCR was run in triplicate using a 7500 Fast Real-Time PCR System (Applied Biosystems), and SDS v1.4 software (Applied Biosystems) was used for comparative ΔC_t analysis. U6 snRNA (RNU6B; Applied Biosystems) served as an endogenous control.

Gene expression microarray analysis

One-color microarray-based gene expression analysis was carried out according to the manufacturer's instructions (Agilent Technologies). Briefly, 700 ng of total RNA were amplified and labeled using a Quick Amp Labeling Kit One-Color (Agilent Technologies), after which the synthesized cRNA was hybridized to the Whole Human Genome Oligo DNA microarray, which includes 41,000 probe sets covering 19,416 genes (G4112F; Agilent Technologies). The microarray data were analyzed using GeneSpring GX version 11 (Agilent Technologies). The Gene Expression Omnibus accession numbers for the microarray data are GSE31802 and GSE32064.

Quantitative RT-PCR of *HOTAIR*

Single-stranded cDNA was prepared using SuperScript III reverse transcriptase (Invitrogen). Quantitative reverse transcriptase PCR (RT-PCR) of *HOTAIR* was carried out using a TaqMan Gene Expression Assay (Assay ID, Hs03296631_m1; Applied Biosystems) and a 7500 Fast Real-Time PCR System (Applied Biosystems). *GAPDH* (Assay ID, Hs99999905_m1; Applied Biosystems) served as an endogenous control.

DNA copy number and chromatin signature analysis

DNA copy number was analyzed using array-based comparative genome hybridization (CGH) as described previously (6). Trimethylated Histone H3 lysine 4 (H3K4me3) was analyzed using chromatin immunoprecipitation (ChIP) as described previously (13, 14). Details of the experimental procedures are provided in the Supplementary Methods.

Published OnlineFirst January 18, 2012; DOI: 10.1158/0008-5472.CAN-11-1803

Transfection of miRNA inhibitors and siRNA molecules

GIST-T1 cells were described previously (15). For inhibition of miR-196a, cells (3×10^5 cells in 6-well plates) were transfected with 100 pmol of Anti-miR miRNA Inhibitors (Ambion) or Anti-miR miRNA Inhibitors Negative Control #1 (Ambion) using Lipofectamine2000 (Invitrogen). For RNA interference (RNAi)-mediated knockdown of *HOTAIR*, 3 different Stealth siRNAs against *HOTAIR* were generated by Invitrogen, after which a mixture of the 3 was used for transfection. Cells (3×10^5 cells in 6-well plates) were transfected with 100 pmol of siRNA or with Stealth RNAi Negative Control Medium GC (Invitrogen) using Lipofectamine2000 (Invitrogen). Total RNA extraction, cell viability assays, and Matrigel invasion assays were carried out 48 hours after transfection as described in the Supplementary Methods.

Statistical analysis

All gene expression levels were log transformed for subsequent statistical analysis because the distribution of expression data seemed to follow a log-normal distribution. Geometric means were therefore calculated as summary statistics for expression levels. Comparisons of continuous variables were made using *t* tests or one-way ANOVA with post hoc multiple comparisons (Games–Howell test). Pearson's correlation coefficients were calculated to describe the strength of the correlation between 2 variables. Comparisons of categorical variables were made using Fisher exact test. To assess the association between prognostic factors and gene expression levels, logistic or Cox regression analyses were carried out. For these regression analyses, the most optimal cutoff points were employed to calculate ORs and HRs, with or without adjustment for clinical factors. Kaplan–Meier curves were plotted to compare 2 groups stratified by gene expression status. All statistical analyses were done using SPSS Statistics 18 (IBM Corporation).

Results

Detection of upregulated miR-196a expression in high-risk GISTs

To examine the miRNA expression signature in GISTs, we carried out miRNA microarray analysis with 32 fresh frozen GIST specimens (10 low-risk, 8 intermediate-risk, and 14 high-risk GISTs). The clinicopathologic features of the 32 patients are listed in Supplementary Table S1. Of 939 probe sets, 470 were excluded because of the absence of a detectable signal in any of the samples tested. Unsupervised hierarchical clustering using the remaining 469 probe sets revealed that GISTs in which there was abundant expression of miRNAs encoded on chromosome 14q32.31 form a separate cluster (Supplementary Figs. S1 and S2). Moreover, by comparing the miRNA expression profiles with array CGH results, we found that this cluster is enriched in tumors without 14q loss. These results are consistent with recent reports showing an inverse relationship between 14q loss and expression of miRNAs located on 14q in GISTs (11, 12), which is indicative of the reliability of our microarray analysis. We next carried out a scatter plot analysis and found that miR-196a is markedly upregulated in high-risk GISTs, as compared with low- or intermediate-risk GISTs (Fig. 1A). As shown in Fig. 1B, miR-196a was undetectable in all but one of the low- and intermediate-risk GISTs tested, whereas it was upregulated in more than half of the high-risk tumors. The elevated expression of miR-196a was observed in both gastric and small intestinal GISTs (Supplementary Table S1).

Upregulation of miR-196a is associated with GIST malignancy

To assess the clinical importance of miR-196a upregulation in GISTs, we next carried out TaqMan assay with 56 fresh frozen GIST specimens (discovery cohort), including the 32 specimens initially analyzed by microarray. The clinicopathologic features of the patients are summarized in Table 1. The TaqMan assay results were highly consistent with the microarray data, though the TaqMan assay did reveal low levels of miR-196a expression in samples in which there was no detectable signal from the microarray (Supplementary Fig. S3).

Also consistent with the microarray results was the finding that miR-196a was markedly upregulated in high-risk GISTs, as compared with the other groups ($P = 0.004$, one-way ANOVA; Fig. 1C, Supplementary Table S2). In addition, logistic regression analysis revealed that the association between miR-196a upregulation and the high-risk category was highest when we employed a cutoff value of miR-196a/U6 0.4 or more (OR = 13.7; 95% CI: 3.4–54.6; $P < 0.001$; Supplementary Table S3). Survival data were obtained for 32 patients, and Cox hazard analysis revealed the highest HR for patients with elevated miR-196a expression when a cutoff value of 1.4 was employed (Table 2). Kaplan–Meier analysis showed poor overall survival among patients with GISTs expressing high levels of miR-196a, though the effect was not statistically significant (Fig. 1D).

We next used TaqMan assay to analyze an independent validation cohort consisting of 100 FFPE GIST specimens (Table 1). Consistent with the findings summarized above, we observed that upregulation of miR-196a was associated with high-risk GISTs (Fig. 1C, Supplementary Tables S2 and S3). By using the same cutoff value (miR-196a/U6 $\geq$ 1.4), Cox hazard analysis revealed an elevated HR for patients exhibiting high levels of miR-196a expression (Table 2), and Kaplan–Meier analysis showed shorter survival times for the same patients (Fig. 1D). These results confirmed the prognostic value of miR-196a expression in both fresh frozen and FFPE GIST specimens.

Finally, we combined the GIST samples in the discovery and validation cohorts to examine the clinicopathologic significance of miR-196a. Expression of miR-196a correlated positively with high-risk grade (Fig. 1C, Supplementary Tables S2 and S3), poor clinical outcome (Fig. 1D, Table 2), tumor size, mitotic count, and metastasis (Table 3). Interestingly, although expression of miR-196a was not associated with age or gender, it was strongly associated with tumor location (Table 3). The median level of miR-196a expression was lowest in specimens from esophageal GISTs and then increased as the GIST site moved from the oral side toward the anal side of the gastrointestinal tract ($P < 0.001$; Table 3, Supplementary Fig. S4). Importantly, although the average level of miR-196a expression was higher in small intestine than in stomach, it was positively

Published OnlineFirst January 18, 2012; DOI: 10.1158/0008-5472.CAN-11-1803

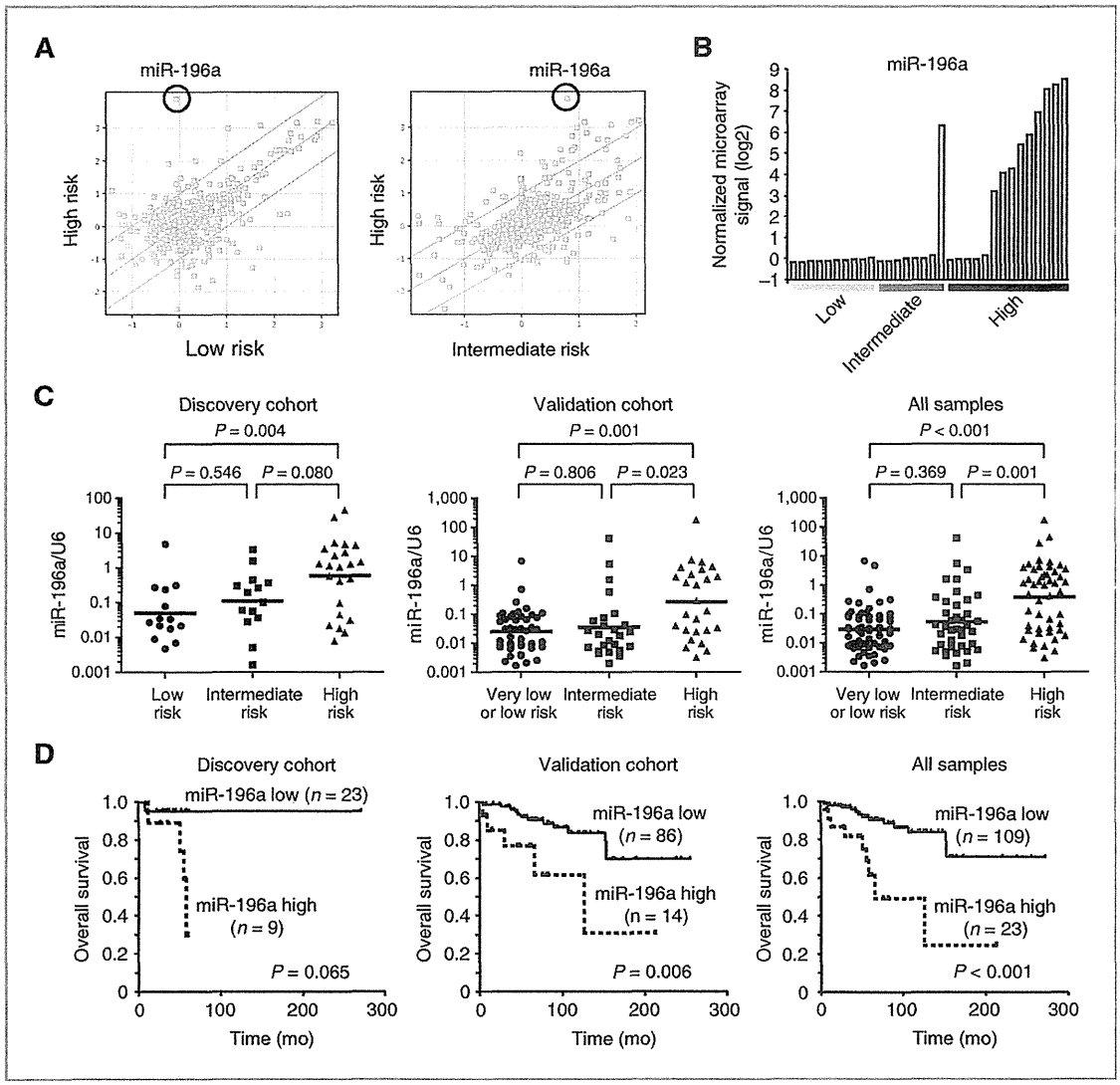

Figure 1. Upregulation of miR-196a expression in GISTs is associated with a high-risk grade and poor prognosis. A, scatter plots analyses: plotting low-risk ($n = 10$) versus high-risk GISTs ($n = 14$; left) and intermediate-risk ($n = 8$) versus high-risk GISTs ($n = 14$; right) revealed overexpression of miR-196a in high-risk GISTs. Microarray data are normalized and log transformed (base 2). Expression of miR-196a is highlighted by a circle. B, levels of miR-196a expression obtained from microarray analysis of 32 GIST specimens. Risk categories are indicated below. C, comparison of miR-196a expression using TaqMan assay in low- ($n = 14$), intermediate- ($n = 14$), and high-risk GISTs ($n = 23$) in a discovery cohort (left), very low- or low-risk ($n = 46$), intermediate-risk ($n = 25$), and high-risk GISTs ($n = 26$) in a validation cohort (middle) and all GIST specimens (right). Results are normalized to internal U6 snRNA. D, Kaplan–Meier curves showing the effect of miR-196a expression (high, miR-196a/U6 $\geq$ 1.4; low, miR-196a/U6 < 1.4) on overall survival in the discovery cohort (left), validation cohort (middle), and all GIST patients (right).

correlated with high-risk grade in both organs (Supplementary Table S4).

Concurrent upregulation of miR-196a and *HOX* cluster genes in GISTs

To analyze the relationship between miR-196a upregulation and the global gene expression profiles in GISTs, we selected age-, gender-, and tumor location–matched GIST specimens showing either low ($n = 7$; average miR-196a/U6 = 0.1) or high miR-196a expression ($n = 7$; average miR-196a/U6 = 15.7) and subjected them to gene expression microarray analysis (Supplementary Table S5). We found that for 4,947 probe sets (corresponding to 3,206 unique genes), there was more than a 2-fold difference in expression between GISTs with miR-196a

Published OnlineFirst January 18, 2012; DOI: 10.1158/0008-5472.CAN-11-1803

Table 1. Clinical features of the GIST samples used in this study

Discovery cohort	
Age (y, median ± SD)	68.0 ± 15.2
Gender	
Male	32 (57.1%)
Female	24 (42.9%)
Tumor location	
Stomach	40 (71.4%)
Small intestine	14 (25.0%)
Omentum	1 (1.8%)
Colorectum	1 (1.8%)
Risk category (n = 51)	
Low	14 (27.5%)
Intermediate	14 (27.5%)
High	23 (45.0%)
Validation cohort	
Age (y, median ± SD)	64.0 ± 12.4
Gender	
Male	44 (44.0%)
Female	56 (56.0%)
Tumor location	
Esophagus	5 (5.2%)
Stomach	84 (84.0%)
Small intestine	8 (8.0%)
Colorectum	3 (3.0%)
Risk category (n = 97)	
Very low	1 (1.0%)
Low	45 (46.4%)
Intermediate	25 (25.8%)
High	26 (26.8%)

overexpression and those without it. Hierarchical clustering analysis using the 4,947 probe sets clearly distinguished between tumors on the basis of their miR-196a expression status (Fig. 2A), and Gene Ontology analysis suggested that genes related to "immune system," "plasma membrane," and "cell communication" are strongly overrepresented among the differentially expressed genes (Supplementary Table S6).

To further characterize the differentially expressed genes, we carried out a gene set analysis and obtained the highest enrichment score with the *HOX* gene set (Supplementary Table S7). We found miR-196a to be encoded at 2 paralogous loci, *miR-196a-1* and *miR-196a-2*, which are located within the *HOXB* and *HOXC* clusters, respectively (Fig. 2B; ref. 16). Hierarchical clustering analysis using the expression data for *HOXC* genes clearly differentiated the GIST samples into 2 groups, and we observed perfect correspondence between higher expression of multiple *HOXC* genes and upregulation of miR-196a (Fig. 2C). By contrast, genes in other *HOX* clusters did not show such obvious correlations with miR-196a (Fig. 2C, Supplementary Fig. S5). We next compared the microarray signal for each *HOX* gene with the miR-196a expression and found strong positive correlations between the expression levels of a number of *HOXC* genes and those of miR-196a (Fig. 3D, Supplementary Fig. S6). Notably, we also found that expression of *HOTAIR*, which encodes a large intergenic noncoding RNA (lincRNA) and is located in an antisense orientation relative to the *HOXC* genes, is concurrently upregulated with miR-196a (Fig. 2C and D). Levels of miR-196a expression also correlated moderately with those of the *HOXB* genes neighboring *miR-196a-1* (*HOXB13* and *HOXB9*), but the correlations were less significant than those with *HOXC* genes (Supplementary Fig. S7).

The similarity between the expression patterns of *HOXC* genes and those of the noncoding RNAs encoded in the same locus is indicative of a common regulatory mechanism involved in the activation of these genes in GISTs. However, array CGH analysis of 27 GIST specimens failed to detect either gain or loss in any *HOX* loci, irrespective of *miR-196a* or *HOX* gene expression, which makes it unlikely that genomic amplification is the cause of their overexpression (Supplementary Fig. S8).

Upregulation of *HOTAIR* is associated with GIST malignancy

A recent study showed that *HOTAIR* is overexpressed in primary breast cancer and is associated with metastasis (17). To examine its clinical significance in GISTs, we carried out TaqMan assays of *HOTAIR* with the discovery cohort samples. We found that the microarray signals for *HOTAIR* were highly

Table 2. miR-196a expression is associated with poor clinical outcome in GIST patients

		Outcome					
	miR-196a/U6	Survival	Death	HR (95% CI)	*P*	HR[a] (95% CI)	*P*
Discovery cohort	<1.4	22	1				
	≥1.4	5	4	6.3 (0.7–57.5)	0.104	32.9 (2.0–551.3)	0.015
Validation cohort	<1.4	73	13				
	≥1.4	9	5	3.9 (1.4–11.1)	0.011	8.4 (2.6–26.9)	<0.001
All samples	<1.4	95	14				
	≥1.4	14	9	4.9 (2.1–11.7)	<0.001	9.1 (3.5–23.7)	<0.001

[a]Age and gender adjusted HR.

Published OnlineFirst January 18, 2012; DOI: 10.1158/0008-5472.CAN-11-1803

Table 3. Correlation between miR-196a expression and clinicopathologic features of GISTs

		miR-196a/U6				
	n	Geometric mean	95% CI	*P*		
Age (y)						
<65	76	0.093	0.051–0.168			
≥65	81	0.074	0.044–0.127	0.581		
Gender						
M	76	0.104	0.059–0.186			
F	80	0.069	0.040–0.119	0.297		
Location						
Esophagus	5	0.019	0.001–0.417	Ref		
Stomach	124	0.061	0.039–0.094	0.741	Ref	
Small intestine	22	0.395	0.163–0.957	0.161	0.002	Ref
Colorectum	4	4.936	2.564–9.502	0.023	<0.001	<0.001
				<0.001		
Tumor size (cm)						
≤5.0	70	0.045	0.026–0.075			
>5.0	81	0.118	0.066–0.210	0.016		
Mitotic count (/50 HPF)						
≤5	105	0.036	0.025–0.053			
>5	35	0.539	0.215–1.353	<0.001		
Metastasis						
Yes	28	0.747	0.307–1.819			
No	108	0.041	0.027–0.063	<0.001		

consistent with the TaqMan assay results (Supplementary Fig. S9). *HOTAIR* was upregulated exclusively in high-risk GISTs, as compared with low- or intermediate-risk GISTs ($P = 0.018$; Fig. 3A), and its expression correlated positively with the expression of miR-196a (Fig. 3B) and *HOXC* genes (Fig. 3C, Supplementary Fig. S10). In addition, logistic regression analysis revealed that high levels of *HOTAIR* expression in GISTs (*HOTAIR*/*GAPDH* ≥ 0.0002) were strongly associated with metastasis (age and gender adjusted OR = 8.2; 95% CI: 1.4–48.4; $P = 0.021$). Cox hazard analysis suggested an elevated HR for patients with high *HOTAIR* expression (Table 4), and Kaplan–Meier analysis showed poor overall survival for the same patients, though the effect was not statistically significant (Fig. 3D). We also tried to analyze *HOTAIR* expression in the FFPE specimens; however, we failed to detect expression of either *HOTAIR* or *GAPDH* in these samples, most likely due to an inadequate quality of the RNA.

Reduced expression of miR-196a and *HOTAIR* target genes in GISTs

To examine the functional role of miR-196a in GISTs, we interrogated our gene expression microarray data for miR-196a target genes computationally predicted by TargetScan. Of the 2,248 genes whose expression was reduced in GISTs overexpressing miR-196a, 95 corresponded to predicted targets (Supplementary Fig. S11, Supplementary Table S8). This gene list included *ANXA1* (Annexin A1), which is an experimentally validated miR-196a target gene (18). In addition, expression of several *HOX* genes, including *HOXB8*, was reduced in GISTs overexpressing miR-196a, which is consistent with an earlier finding of miR-196a–directed cleavage of *HOXB8* mRNA (Supplementary Fig. S11; ref. 19).

In normal human fibroblasts, *HOTAIR* represses *HOXD* gene expression by interacting with polycomb repressive complex 2 (PRC2; ref. 20). In breast cancer cells, overexpression of *HOTAIR* was shown to recruit PRC2 to more than 800 gene promoters, leading to histone H3K27 methylation and epigenetic silencing of the target genes (17). We therefore examined our microarray data for the reported *HOTAIR*-induced PRC2 target genes. Among 14 GISTs analyzed with the microarray, all 7 tumors strongly expressing miR-196a showed elevated *HOTAIR* expression (average *HOTAIR*/*GAPDH* = 0.00254), whereas all tumors only weakly expressing miR-196a showed little or no *HOTAIR* expression (average *HOTAIR*/*GAPDH* = 0.00001). We found that expression of 144 *HOTAIR* target genes was reduced in GISTs overexpressing *HOTAIR* (Supplementary Fig. S11, Supplementary Table S9). These results indicated that overexpression of miR-196a and *HOTAIR* may contribute to the malignant progression of GISTs by modulating expression of their target genes.

Inhibition of *miR-196a* and *HOTAIR* suppresses GIST cell invasion

We next utilized a cultured GIST cell line to determine whether upregulation of miR-196a and *HOTAIR* is responsible for the malignant potential of GISTs. We found that both

Published OnlineFirst January 18, 2012; DOI: 10.1158/0008-5472.CAN-11-1803

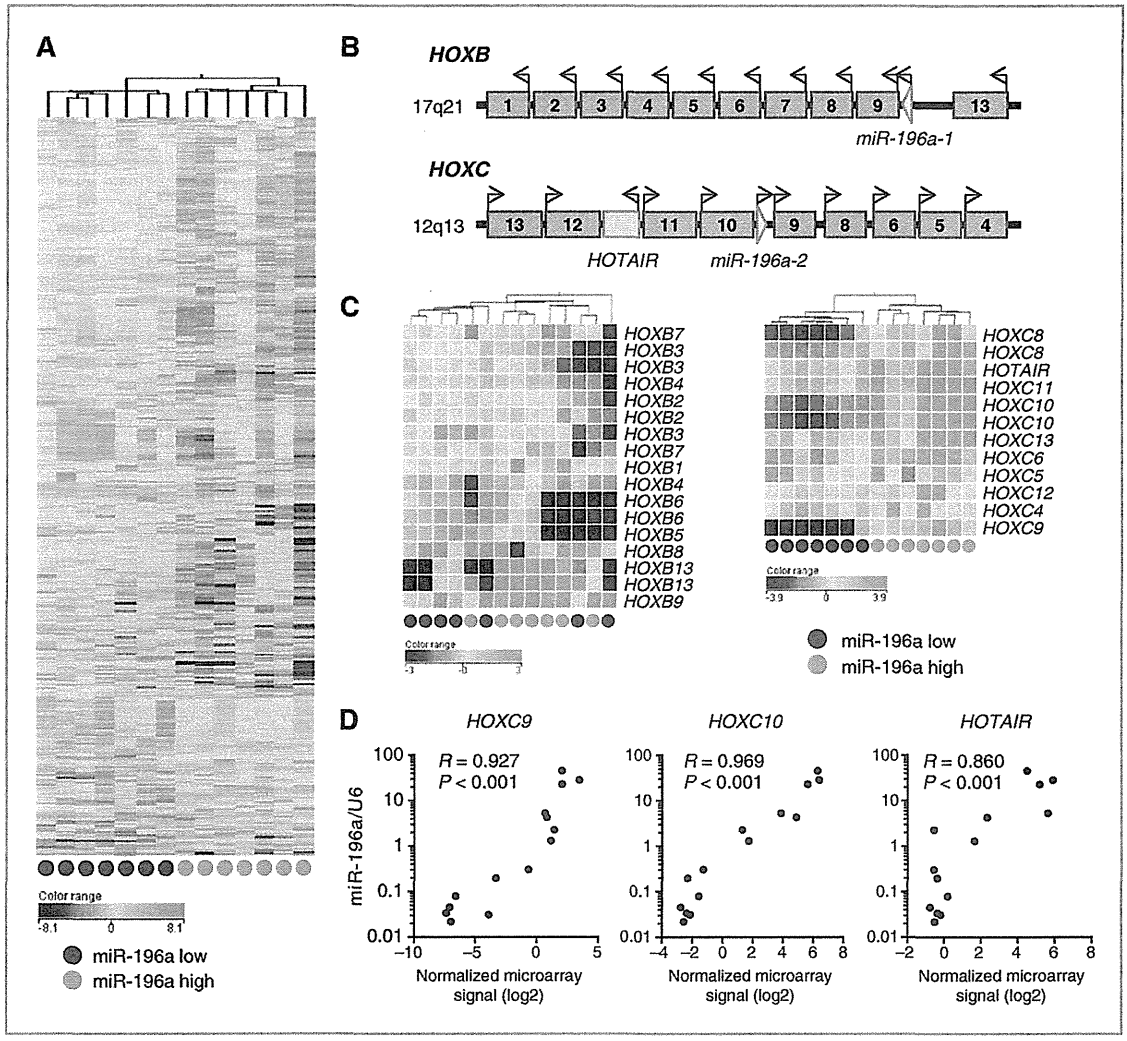

Figure 2. *GIST* gene expression signatures reveal a strong correlation between the *miR-196a* and *HOXC* genes. A, heat map of the gene expression signatures correlated with miR-196a expression. Rows represent probe sets and columns represent patients. A total of 4,947 probe sets differentially expressed (>2-fold change) between GISTs with ($n = 7$) and without ($n = 7$) miR-196a overexpression were selected, after which hierarchical clustering was carried out. The miR-196a expression status is indicated below. B, schematic representations of the *miR-196a* family locations within the *HOX* gene clusters. C, hierarchical clustering analysis using *HOXB* (left) and *HOXC* (right) expression data. miR-196a expression status is indicated below. D, correlations between the expression levels of miR-196a and *HOXC* genes or *HOTAIR*. Expression of miR-196a was analyzed using TaqMan assay and was normalized to internal U6 snRNA. Microarray data for *HOXC* and *HOTAIR* were normalized and log transformed (base 2). The Pearson correlation coefficients and *P* values are shown.

miR-196a and *HOTAIR* are expressed in GIST-T1 cells (Supplementary Fig. S12). We then carried out cell viability and Matrigel invasion assays after transfecting GIST-T1 cells with an anti–miR-196a inhibitor molecule. Gene expression microarray analysis revealed that a number of predicted miR-196a target genes, including *ANXA1* and *HOXA5*, were upregulated by inhibition of miR-196a (Supplementary Table S10), and although we observed no effects on cell viability, inhibition of miR-196a moderately suppressed cell invasion (Supplementary Fig. S13). We next disrupted *HOTAIR* expression by transfecting the cells with siRNAs targeting it (Fig. 3E). Although knockdown of *HOTAIR* did not significantly affect cell viability, it suppressed the invasiveness of GIST-T1 cells (Fig. 3E and F). Moreover, gene expression microarray analysis revealed that a number of reported *HOTAIR* target genes, including *PCHD10*, *SEMA6A*, and *STK17B*, were upregulated upon knockdown of *HOTAIR* (Supplementary Table S11). In all, we found that 1,424 genes were upregulated by siHOT (>2-fold), and Gene Ontology analysis revealed enrichment of genes related to "nucleus," "chromosome," and "membrane-bounded

Published OnlineFirst January 18, 2012; DOI: 10.1158/0008-5472.CAN-11-1803

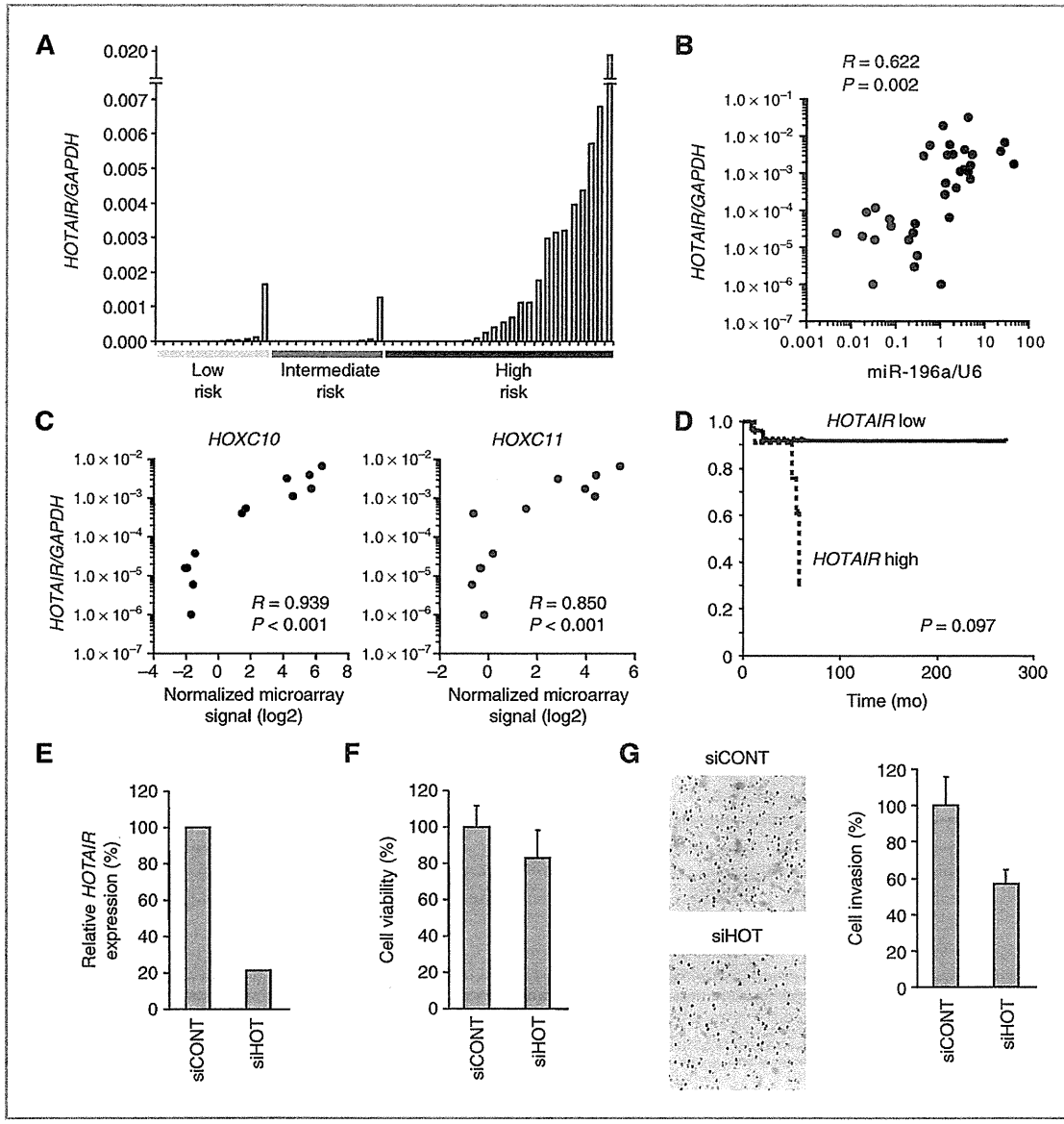

Figure 3. Upregulation of *HOTAIR* in malignant GISTs. A, TaqMan assay of *HOTAIR* in a panel of GIST specimens ($n = 52$). Results are normalized to internal *GAPDH* expression. Risk categories are indicated below. B, correlation between levels of *HOTAIR* and miR-196a expression detected using TaqMan assay. The Pearson correlation coefficient and *P* value are shown. C, correlations between levels of *HOTAIR* expression detected using TaqMan assay and those of *HOXC* genes detected from microarrays. The Pearson correlation coefficients and *P* values are shown. D, Kaplan–Meier curves showing the effect of *HOTAIR* expression (high, *HOTAIR/GAPDH* $\geq$ 0.0002; low, *HOTAIR/GAPDH* < 0.0002) on overall survival among GIST patients. E, TaqMan assay for *HOTAIR* in GIST-T1 cells transfected with control siRNA (siCONT) or siRNA targeting *HOTAIR* (siHOT). F, cell viability assay using GIST-T1 cells transfected with siCONT or siHOT. Cell viabilities were determined 48 hours after transfection. Shown are the means of 8 replications; error bars represent SDs. G, Matrigel invasion assay using GIST-T1 cells transfected with siCONT or siHOT. Shown on the right are the means of 3 random microscopic fields per membrane; error bars represent SDs.

organelle" (Supplementary Tables S12 and S13). These results suggested that *HOTAIR* may modulate transcription of a large number of genes and may have previously unidentified roles in GIST cells.

Finally, we sought to clarify the biologic relationship between miR-196a, *HOTAIR*, and *HOXC* genes. We first tested whether upregulation of miR-196a is a downstream effect of *HOTAIR* dysregulation, or vice versa. We found that inhibition

Published OnlineFirst January 18, 2012; DOI: 10.1158/0008-5472.CAN-11-1803

Table 4. HOTAIR expression is associated with poor clinical outcome in GIST patients

	Outcome					
HOTAIR/GAPDH	**Survival**	**Death**	**HR (95% CI)**	***P***	**HR[a] (95% CI)**	***P***
<0.0002	26	2				
≥0.0002	7	4	3.8 (0.7–21.2)	0.123	9.0 (1.2–68.9)	0.034

[a]Age and gender adjusted HR.

of miR-196a had no effect on *HOTAIR* expression in GIST-T1 cells, nor did knockdown of *HOTAIR* affect miR-196a expression. This suggested that overexpression of miR-196a or *HOTAIR* is not a simple downstream effect of their dysregulation (Supplementary Fig. S12). By contrast, analysis of the chromatin status in GIST-T1 cells using ChIP-PCR revealed enrichment of trimethylated histone H3 lysine 4 (H3K4me3), a hallmark of active gene transcription, at the transcription start sites of multiple *HOXC* genes and *HOTAIR* (Supplementary Fig. S14). Moreover, we found concurrent overexpression of miR-196a, *HOTAIR*, and *HOXC* genes in other cancer cells, including the KatoIII gastric cancer cell line. By carrying out high-resolution ChIP-seq analysis with the KatoIII cells, we observed significant enrichment of H3K4me3 over a wide range (more than 50 kb) of the *HOXC* cluster, which suggested that an epigenetic mechanism is involved in the dysregulation of this genomic region (Supplementary Fig. S15).

Discussion

Although the results of recent studies suggest that the gene expression signatures of GISTs are predictive of malignancy and drug sensitivity of the tumors (5, 21), the clinical significance of the miRNA expression signature is not yet fully understood. In this study, we found that upregulation of miR-196a is strongly associated with a high-risk grade, metastasis, and poor prognosis in GIST patients. Furthermore, overexpression of miR-196a is accompanied by upregulation of multiple *HOXC* genes and the metastasis-related lincRNA *HOTAIR*. To our knowledge, this is the first article to show concurrent overexpression of collinear *HOX* genes and noncoding RNAs in human malignancy.

A number of studies have implicated miR-196a in malignancy, but its role may differ among tumor types. Upregulation of miR-196a is observed in esophageal adenocarcinomas and their precancerous lesions, Barrett's esophagus and dysplasia, which suggests miR-196a is a potential marker of the malignant progression of Barrett's esophagus (22). Strong expression of miR-196a is also associated with a poor prognosis in pancreatic adenocarcinoma and glioblastoma patients (23, 24). In addition, functional analysis showed that expression of miR-196a in esophageal, breast, and endometrial cancer cells promotes proliferation and suppresses apoptosis through downregulation of *ANXA1* (18). These results suggest that miR-196a contributes to oncogenesis in cancer. On the other hand, miR-196a is significantly downregulated in melanoma, and its reexpression inhibited the invasive behavior of melanoma cells by targeting HOXC8 (25). Similarly, miR-196a suppressed HOXC8 and inhibited invasion and metastasis by breast cancer cells (26). Thus miR-196a seems to exert opposite effects in tumors of different origins.

The *HOX* genes are a highly conserved subgroup of the homeobox superfamily, and they play essential roles in a variety of biologic processes, including development, differentiation, apoptosis, and angiogenesis (27). In humans, 4 *HOX* clusters containing 39 *HOX* genes have been identified, and dysregulation of their expression is observed in various malignancies. Although the role of HOXs in cancer is not fully understood, its aberrant expression is thought to affect pathways that promote tumorigenesis and metastasis (27). For instance, *HOXC8* mRNA is overexpressed in prostate cancer cells and is associated with tumor cell proliferation and metastasis (28–30). In addition, *HOXC5* and *HOXC8* mRNAs are upregulated in cervical cancer cells (31), and one recent study suggested HOXC10 plays a key role of in the progression and invasion in cervical cancer (32).

An association between miR-196a and *HOX* expression in cancer has also been reported. Reduced expression of miR-196a in malignant melanoma cells leads to upregulation of HOXB7 and, in turn, activation of BMP4, a major modulator of migration (33). As mentioned above, miR-196a also inhibits invasion and metastasis by downregulating HOXC8 in melanoma and breast cancer cells (26, 34). Taken together, these results suggest that miR-196a acts as a tumor suppressor by targeting *HOX* genes in these tumor types. By contrast, we show in this study that both the miR-196a and *HOXC* genes are concurrently upregulated in malignant GISTs. Our findings are reminiscent of an earlier report showing that the expression patterns of miRNAs embedded in *HOX* clusters are very similar to those of *HOX* genes during mammalian embryogenesis (35). Global gene expression analysis revealed that expression of multiple putative miR-196a targets, including *ANXA1*, is diminished in GISTs overexpressing miR-196a, whereas their expression is enhanced upon inhibition of miR-196a in cultured GIST-T1 cells. In addition, inhibition of miR-196a in GIST cells overexpressing that miRNA moderately suppressed cell invasion. Taken together, our results indicate that upregulation of *HOXC* genes along with miR-196a may contribute to the malignant potential of GIST.

HOTAIR is located within the *HOXC* cluster and encodes a lincRNA known to repress its target genes by directly interacting with histone modification complexes. Epigenetic gene

Published OnlineFirst January 18, 2012; DOI: 10.1158/0008-5472.CAN-11-1803

regulation is closely associated with histone modifications in which di- or trimethylation of histone H3 lysine 4 (H3K4me2 or H3K4me3) is enriched within active gene promoters. In addition, trimethylation of histone H3 lysine 27 (H3K27me3) is a marker of gene silencing. In normal adult fibroblasts, *HOTAIR* suppresses the *HOXD* locus by recruiting the PRC2 complex, which consists of the histone H3K27 methylase EZH2, SUZ12, and EED (20). It was also recently shown that *HOTAIR* serves as a scaffold for multiple repressor complexes, including PRC2 and LSD1/CoREST/REST (36). LSD1 is a demethylase that specifically mediates demethylation of H3K4, leading to repression of the target genes. *HOTAIR* is also strongly implicated in cancer metastasis. In breast cancer cells, *HOTAIR* induces retargeting of the PRC2 complex throughout the genome, which leads to the silencing of multiple tumor suppressor and metastasis suppressor genes (17). Overexpression of *HOTAIR* is also predictive of recurrence in hepatocellular carcinoma patients after liver transplantation (37). We observed that upregulation of *HOTAIR* is closely associated with GIST aggressiveness and metastasis. In addition, functional analysis using GIST-T1 cells showed that RNAi-mediated knockdown of *HOTAIR* suppressed cell invasion. These results strongly suggest that upregulation of *HOTAIR* is one of the mechanisms that promote aggressiveness in GISTs. Interestingly, depletion of *HOTAIR* induced a significant change in the gene expression profile in GIST cells, suggesting that *HOTAIR* may regulate a spectrum of genes other than the previously reported target genes. Further studies, including genome-wide histone modification analysis, may reveal as yet unidentified roles played by *HOTAIR* in the malignant progression of GISTs.

The mechanism underlying upregulation of *HOX* cluster genes and noncoding RNAs in GISTs is intriguing. Our array CGH analysis did not detect chromosomal aberrations in any *HOX* loci, making it unlikely that gene amplification is the cause of their overexpression. However, we found that the transcription start sites of multiple genes in the *HOXC* cluster are marked by an active histone mark, H3K4me3, in GIST-T1 cells. Moreover, high-resolution ChIP-seq analysis revealed that, in cancer cells, the entire region is significantly enriched with H3K4me3, leading to overexpression of the affected genes. Our results are reminiscent of the recent finding that rearrangement of *MLL* in leukemia induces active histone modifications at the promoters of *HOXA* genes and miR-196b, resulting to their overexpression (38–40). Although such rearrangements are not known in GISTs, further study to clarify the involvement of epigenetic modifiers in malignant GISTs may lead to identification of new therapeutic targets.

Overall, our study has shown that noncoding RNAs encoded in the *HOXC* cluster could be useful predictive markers as well as novel therapeutic targets in malignant GISTs. As miRNAs are well preserved in FFPE specimens (41), miR-196a could be a reliable biomarker for risk assessment. We also provide evidence that *HOTAIR* is significantly upregulated in high-risk GISTs, indicating that this lincRNA also could be a useful biomarker, as well as a novel therapeutic target. Further study of the causes and functions of *HOXC* locus activation in GISTs may provide new strategies for the treatment of GIST patients.

Disclosure of Potential Conflicts of Interest

T. Nishida has received a research grant from Novartis Pharma K.K. The remaining authors disclose no conflicts of interest.

Acknowledgments

The authors thank Dr. William F. Goldman for editing the manuscript and M. Ashida for technical assistance.

Grant Support

This study was supported in part by grants-in-aid for Scientific Research (B) from the Japan Society for Promotion of Science (Y. Shinomura), A3 foresight program from the Japan Society for Promotion of Science (H. Suzuki), a grant-in-aid for the Third-term Comprehensive 10-year Strategy for Cancer Control (M. Toyota, H. Suzuki), a grant-in-aid for Cancer Research from the Ministry of Health, Labor, and Welfare, Japan (M. Toyota, H. Suzuki), and the Takeda Science Foundation (H. Suzuki).

The costs of publication of this article were defrayed in part by the payment of page charges. This article must therefore be hereby marked *advertisement* in accordance with 18 U.S.C. Section 1734 solely to indicate this fact.

Received May 31, 2011; revised December 19, 2011; accepted January 6, 2012; published OnlineFirst January 18, 2012.

References

1. Shinomura Y, Kinoshita K, Tsutsui S, Hirota S. Pathophysiology, diagnosis, and treatment of gastrointestinal stromal tumors. J Gastroenterol 2005;40:775–80.
2. Rubin BP, Heinrich MC, Corless CL. Gastrointestinal stromal tumour. Lancet 2007;369:1731–41.
3. Corless CL, Fletcher JA, Heinrich MC. Biology of gastrointestinal stromal tumors. J Clin Oncol 2004;22:3813–25.
4. Fletcher CD, Berman JJ, Corless C, Gorstein F, Lasota J, Longley BJ, et al. Diagnosis of gastrointestinal stromal tumors: A consensus approach. Hum Pathol 2002;33:459–65.
5. Yamaguchi U, Nakayama R, Honda K, Ichikawa H, Hasegawa T, Shitashige M, et al. Distinct gene expression-defined classes of gastrointestinal stromal tumor. J Clin Oncol 2008;26:4100–8.
6. Igarashi S, Suzuki H, Niinuma T, Shimizu H, Nojima M, Iwaki H, et al. A novel correlation between LINE-1 hypomethylation and the malignancy of gastrointestinal stromal tumors. Clin Cancer Res 2010;16:5114–23.
7. He L, Hannon GJ. MicroRNAs: small RNAs with a big role in gene regulation. Nat Rev Genet 2004;5:522–31.
8. Esquela-Kerscher A, Slack FJ. Oncomirs–microRNAs with a role in cancer. Nat Rev Cancer 2006;6:259–69.
9. Croce CM. Causes and consequences of microRNA dysregulation in cancer. Nat Rev Genet 2009;10:704–14.
10. Calin GA, Croce CM. MicroRNA signatures in human cancers. Nat Rev Cancer 2006;6:857–66.
11. Choi HJ, Lee H, Kim H, Kwon JE, Kang HJ, You KT, et al. MicroRNA expression profile of gastrointestinal stromal tumors is distinguished by 14q loss and anatomic site. Int J Cancer 2010;126:1640–50.
12. Haller F, von Heydebreck A, Zhang JD, Gunawan B, Langer C, Ramadori G, et al. Localization- and mutation-dependent microRNA (miRNA) expression signatures in gastrointestinal stromal tumours (GISTs), with a cluster of co-expressed miRNAs located at 14q32.31. J Pathol 2010;220:71–86.
13. Maruyama R, Choudhury S, Kowalczyk A, Bessarabova M, Beresford-Smith B, Conway T, et al. Epigenetic regulation of cell type-specific expression patterns in the human mammary epithelium. PLoS Genet 2011;7:e1001369.
14. Suzuki H, Takatsuka S, Akashi H, Yamamoto E, Nojima M, Maruyama R, et al. Genome-wide profiling of chromatin signatures reveals epigenetic regulation of microRNA genes in colorectal cancer. Cancer Res 2011;71:5646–58.

Published OnlineFirst January 18, 2012; DOI: 10.1158/0008-5472.CAN-11-1803

15. Taguchi T, Sonobe H, Toyonaga S, Yamasaki I, Shuin T, Takano A, et al. Conventional and molecular cytogenetic characterization of a new human cell line, GIST-T1, established from gastrointestinal stromal tumor. Lab Invest 2002;82:663–5.
16. Calin GA, Sevignani C, Dumitru CD, Hyslop T, Noch E, Yendamuri S, et al. Human microRNA genes are frequently located at fragile sites and genomic regions involved in cancers. Proc Natl Acad Sci U S A 2004;101:2999–3004.
17. Gupta RA, Shah N, Wang KC, Kim J, Horlings HM, Wong DJ, et al. Long non-coding RNA HOTAIR reprograms chromatin state to promote cancer metastasis. Nature 2010;464:1071–6.
18. Luthra R, Singh RR, Luthra MG, Li YX, Hannah C, Romans AM, et al. MicroRNA-196a targets annexin A1: a microRNA-mediated mechanism of annexin A1 downregulation in cancers. Oncogene 2008;27:6667–78.
19. Yekta S, Shih IH, Bartel DP. MicroRNA-directed cleavage of HOXB8 mRNA. Science 2004;304:594–6.
20. Rinn JL, Kertesz M, Wang JK, Squazzo SL, Xu X, Brugmann SA, et al. Functional demarcation of active and silent chromatin domains in human HOX loci by noncoding RNAs. Cell 2007;129:1311–23.
21. Rink L, Skorobogatko Y, Kossenkov AV, Belinsky MG, Pajak T, Heinrich MC, et al. Gene expression signatures and response to imatinib mesylate in gastrointestinal stromal tumor. Mol Cancer Ther 2009;8:2172–82.
22. Maru DM, Singh RR, Hannah C, Albarracin CT, Li YX, Abraham R, et al. MicroRNA-196a is a potential marker of progression during Barrett's metaplasia-dysplasia-invasive adenocarcinoma sequence in esophagus. Am J Pathol 2009;174:1940–8.
23. Bloomston M, Frankel WL, Petrocca F, Volinia S, Alder H, Hagan JP, et al. MicroRNA expression patterns to differentiate pancreatic adenocarcinoma from normal pancreas and chronic pancreatitis. JAMA 2007;297:1901–8.
24. Guan Y, Mizoguchi M, Yoshimoto K, Hata N, Shono T, Suzuki SO, et al. MiRNA-196 is upregulated in glioblastoma but not in anaplastic astrocytoma and has prognostic significance. Clin Cancer Res 2010;16:4289–97.
25. Mueller DW, Bosserhoff AK. MicroRNA miR-196a controls melanoma-associated genes by regulating HOX-C8 expression. Int J Cancer 2011;129:1064–74.
26. Li Y, Zhang M, Chen H, Dong Z, Ganapathy V, Thangaraju M, et al. Ratio of miR-196s to HOXC8 messenger RNA correlates with breast cancer cell migration and metastasis. Cancer Res 2010;70:7894–904.
27. Shah N, Sukumar S. The Hox genes and their roles in oncogenesis. Nat Rev Cancer 2010;10:361–71.
28. Waltregny D, Alami Y, Clausse N, de Leval J, Castronovo V. Overexpression of the homeobox gene HOXC8 in human prostate cancer correlates with loss of tumor differentiation. Prostate 2002;50:162–9.
29. Miller GJ, Miller HL, van Bokhoven A, Lambert JR, Werahera PN, Schirripa O, et al. Aberrant HOXC expression accompanies the malignant phenotype in human prostate. Cancer Res 2003;63:5879–88.
30. Kikugawa T, Kinugasa Y, Shiraishi K, Nanba D, Nakashiro K, Tanji N, et al. PLZF regulates Pbx1 transcription and Pbx1-HoxC8 complex leads to androgen-independent prostate cancer proliferation. Prostate 2006;66:1092–9.
31. Alami Y, Castronovo V, Belotti D, Flagiello D, Clausse N. HOXC5 and HOXC8 expression are selectively turned on in human cervical cancer cells compared to normal keratinocytes. Biochem Biophys Res Commun 1999;257:738–45.
32. Zhai Y, Kuick R, Nan B, Ota I, Weiss SJ, Trimble CL, et al. Gene expression analysis of preinvasive and invasive cervical squamous cell carcinomas identifies HOXC10 as a key mediator of invasion. Cancer Res 2007;67:10163–72.
33. Braig S, Mueller DW, Rothhammer T, Bosserhoff AK. MicroRNA miR-196a is a central regulator of HOX-B7 and BMP4 expression in malignant melanoma. Cell Mol Life Sci 2010;67:3535–48.
34. Mueller DW, Bosserhoff AK. MicroRNA miR-196a controls melanoma-associated genes by regulating HOX-C8 expression. Int J Cancer 2011;129:1064–74.
35. Mansfield JH, Harfe BD, Nissen R, Obenauer J, Srineel J, Chaudhuri A, et al. MicroRNA-responsive 'sensor' transgenes uncover Hox-like and other developmentally regulated patterns of vertebrate microRNA expression. Nat Genet 2004;36:1079–83.
36. Tsai MC, Manor O, Wan Y, Mosammaparast N, Wang JK, Lan F, et al. Long noncoding RNA as modular scaffold of histone modification complexes. Science 2010;329:689–93.
37. Yang Z, Zhou L, Wu LM, Lai MC, Xie HY, Zhang F, et al. Overexpression of long non-coding RNA HOTAIR predicts tumor recurrence in hepatocellular carcinoma patients following liver transplantation. Ann Surg Oncol 2011;18:1243–50.
38. Okada Y, Feng Q, Lin Y, Jiang Q, Li Y, Coffield VM, et al. hDOT1L links histone methylation to leukemogenesis. Cell 2005;121:167–78.
39. Krivtsov AV, Feng Z, Lemieux ME, Faber J, Vempati S, Sinha AU, et al. H3K79 methylation profiles define murine and human MLL-AF4 leukemias. Cancer Cell 2008;14:355–68.
40. Popovic R, Riesbeck LE, Velu CS, Chaubey A, Zhang J, Achille NJ, et al. Regulation of mir-196b by MLL and its overexpression by MLL fusions contributes to immortalization. Blood 2009;113:3314–22.
41. Hui AB, Shi W, Boutros PC, Miller N, Pintilie M, Fyles T, et al. Robust global micro-RNA profiling with formalin-fixed paraffin-embedded breast cancer tissues. Lab Invest 2009;89:597–606.

Cancer Science
The official journal of the Japanese Cancer Association JCA

Insulin-like growth factor receptor expression is associated with aggressive phenotypes and has therapeutic activity in biliary tract cancers

Hirokazu Ohashi,[1] Yasushi Adachi,[1,4] Hiroyuki Yamamoto,[1] Hiroaki Taniguchi,[1] Katsuhiko Nosho,[1] Hiromu Suzuki,[1] Yoshiaki Arimura,[1] Kohzoh Imai,[2] David P. Carbone[3] and Yasuhisa Shinomura[1]

[1]First Department of Internal Medicine, Sapporo Medical University, Sapporo; [2]Institute of Medical Science, University of Tokyo, Tokyo, Japan; [3]Vanderbilt-Ingram Cancer Center and Departments of Medicine and Cell Biology, Vanderbilt University, Nashville, TN, USA

(Received August 18, 2011/Revised October 21, 2011/Accepted October 24, 2011/Accepted manuscript online November 2, 2011/Article first published online December 13, 2011)

Insulin-like growth factor (IGF)-I receptor (IGF-IR) signaling is required for carcinogenicity and progression of several cancers but the function of this pathway and its utility as a therapeutic target have not been studied comprehensively in biliary tract carcinomas (BTC). We investigated the immunohistochemical expression of elements of the IGF axis, matrilysin, overexpression of p53 and the methylation status of the IGFBP-3 promoter in 80 surgically resected BTC. We also assessed the effect of IGF-IR blockade on signal transduction, proliferation and survival in three BTC cell lines using a new tyrosine kinase inhibitor, BMS-536924, and dominant negative IGF-IR (IGF-IR/dn). The effects of IGF-IR blockade was also studied in nude mouse xenograft models. IGF-I was expressed in 60% and IGF-II in 50% of tumors. High expression was associated with tumor size. IGF-IR was expressed in 69% of the cases and was associated with advanced stage and matrilysin expression. Hypermethylation of the IGFBP-3 promoter was detected in 41% of BTC and was inversely correlated with p53 expression. BMS-536924 blocked autophosphorylation of IGF-IR and both Akt and ERK activation by both IGF-I and insulin. BMS-536924 suppressed proliferation and tumorigenicity *in vitro* in a dose-dependent fashion. This inhibitor upregulated chemotherapy-induced apoptosis in a dose-dependent fashion. Moreover, IGF-IR blockade was effective against tumors in mice. IGF-IR might identify a subset of BTC with a particularly aggressive phenotype and is a candidate therapeutic target in this disease. BMS-536924 might have significant therapeutic utility. (*Cancer Sci* 2012; 103: 252–261)

Biliary tract carcinomas (BTC) have one of the worst outcomes of all malignancies in Asia, Europe and the USA. Owing to its non-specific presenting symptoms, BTC is generally diagnosed late in the disease course.[1] Complete surgical resection is the only curative treatment for BTC, but surgery is often not possible for these advanced diseases.[2–4] Therefore, we must to seek new therapeutic options for this disease.

Recent advances in molecular cancer research have brought new therapeutic strategies targeting these signals into routine clinical usage. Growth factor receptors are one such group of targets and their activity can be blocked by tyrosine kinase inhibitors (TKI) or mAb. Insulin-like growth factor (IGF)-I receptor (IGF-IR) is one such candidate molecular target.[5,6]

Binding of the ligands IGF-I and IGF-II to IGF-IR causes receptor autophosphorylation and activates multiple signaling pathways, including ERK and the phosphatidylinositide 3-kinase (PI3-K)/Akt-1 axis.[7] Activation of IGF-IR is regulated by multiple factors, including IGF binding proteins (IGFBP) and IGF-2 receptors.[8–10]

Dysregulation of the IGF system has been implicated in the proliferation of numerous neoplasms.[6,11] Mutations or chromosomal amplifications of IGF-IR are rare; however, the regulation of IGF-IR expression is closely associated with the function of several oncogenes and tumor suppressor genes.[11] Although wild-type p53 inhibits IGF-IR expression, mutant p53 can induce IGF-IR expression.[12] Elevation of serum IGF-I increases the risk of developing several cancers.[9] IGF-IR signaling is also important in tumor dissemination through the control of migration, angiogenesis, invasion and metastasis.[13,14] The findings outlined above suggest a potential basis for tumor selectivity in therapeutic applications in gastrointestinal cancers.

There is, however, only limited information about the IGF/IGF-IR axis in BTC. In immunohistochemical studies, gallbladder carcinoma (GBC) expressed IGF-I in 45%, IGF-II in 25% and IGF-IR in 95% of cases with BTC[15] and all intrahepatic cholangiocarcinomas expressed both IGF-I and IGF-IR.[16] Several human BTC cells express IGF-IR.[16–18]

IGFBP-3, which is the most abundant IGFBP in the circulation, has both IGF-dependent and IGF-independent antiproliferative and proapoptotic effects on several cancers.[19] IGFBP-3 promoter methylation and gene silencing have been reported in cancers.[20,21] IGFBP-3 is induced by wild-type p53,[22] and promoter methylation at the p53 regulatory element causes gene silencing resistant to p53.[23] Thus, it is important to analyze the relationship between IGFBP-3 promoter methylation and expression of IGF-IR, its ligands and p53 in BTC.

The insulin receptor (InsR) is also a key component of the IGF system. InsR activation leads cell proliferation in addition to glucose metabolism. In addition to insulin, InsR can bind IGF-II and initiate mitogenic signaling.[24] IGF-IR and InsR can form hybrid receptors that bind IGF at physiologic concentrations. InsR and IGF-IR/InsR hybrid receptors might also be involved in cancer biology as both insulin and IGF-I contribute to the development and progression of adenomatous polyps.[25]

We have reported that matrix metalloproteinase-7 (MMP-7, matrilysin) plays a key role in the progression of BTC.[26] Active MMP-7 is correlated with depth of invasion and advanced stage and downregulation of MMP-7 expression by siRNA results in a significant decrease *in vitro* invasiveness. Matrilysin is distinguished from other MMP by several unique characteristics: broad spectrum of proteolytic activity; ability to activate other MMP; and production by cancer cells but not stromal cells.[27,28] Moreover, we have reported a positive feedback loop between the IGF/IGF-IR axis and matrilysin in the progression and invasiveness of gastrointestinal cancers.[13]

Several possible approaches to blocking IGF-IR signaling have been reported. Humanized mAbs are available for IGF-IR,[29,30] and some are in clinical trials. TKI for IGF-IR have

[4]To whom correspondence should be addressed.
E-mail: yadachi@sapmed.ac.jp.

doi: 10.1111/j.1349-7006.2011.02138.x

been developed, including NVP-AEW541.[31] The orally available compound BMS-536924, 1H-(benzimidazol-2-yl)-1H-pyridin-2-one, is a novel TKI for IGF-IR/InsR.[32,33] We have also constructed two dominant negative inhibitors for IGF-IR (IGF-IR/dn; IGF-IR/482st and IGF-IR/950st), which are active as plasmids and recombinant adenovirus vectors in gastrointestinal malignancies.[34–37] IGF-IR/482st encodes a truncated extracellular domain of IGF-IR and, therefore, should result in a secreted form that affects neighboring cells in addition to the transduced cells (a bystander effect).

In the present study, we analyzed the IGF axis in human BTC and assessed the impact of IGF-IR blockade on growth, apoptosis induction and *in vivo* therapeutic efficacy in subcutaneous xenografts.

Materials and Methods

Materials, cell lines, mice and tissue samples. Anti-Akt1 (c-20), anti-ERK1(K-23), anti-phospho-ERK1(E-4), ant-IGF-I(G-17) and anti-IGF-IRβ(C20) were purchased from Santa Cruz Biotechnology (Santa Cruz, CA, USA) and anti-phospho-Akt (Ser473) and anti-phospho-p44/42-MAPK(Thy202/Tyr204) were obtained from Cell-Signaling Technology (Beverly, MA, USA). Cisplatin and 5-fluorouracil (5-FU) were purchased from Sigma (St. Louis, MO, USA). Recombinant human IGF-I was purchased from R&D systems (Minneapolis, MN, USA). Human GBC cell lines TGBC-1TKB, TGBC-2TKB and TGBC-14TKB, and bile duct cancer cell lines TFK-1, HuH-28, MEC and TKKK were obtained from Riken Bioresource Center Cell Bank (Tsukuba, Japan). Cells were cultured in RPMI1640 or DMEM supplemented with 5–10% fetal bovine serum. Specific-pathogen-free female BALB/cAnNCrj-nu mice, 6-weeks-old, were purchased from Charles River (Yokohama, Japan). Mice were cared for and used according to our university's guidelines.

Formalin-fixed, paraffin-embedded sections of 80 BTC (30 GBC, 30 extrahepatic bile duct carcinomas [BDC] and 20 carcinomas of the ampulla of Vater [CAV]) were used for immunohistochemical staining. All tumor specimens were obtained from patients who had undergone surgical treatment at Sapporo Medical University Hospital and affiliated hospitals. Sections containing the most invasive part of each tumor were used. Specimens for real-time PCR were immediately frozen in liquid nitrogen at the time of surgery and stored at −80°C. Histopathological features of the specimens were classified according to the seventh edition of the TNM classification system of the International Union Against Cancer. Informed consent was obtained from each subject. This study was approved by the Institutional Review Board of our university (Institutional Review Board approval number 22-135) and written informed consent was obtained from each subject.

BMS-536924 was kindly provided by Bristol-Myers Squibb (New York, NY, USA). Stock solution was prepared in DMSO and stored at −20°C. For oral administration to rodents, BMS-536924 was dissolved in a mixture of polyethylene glycol 400 (PEG400/water, 4:1 vol/vol) facilitated by stirring through the duration of dosing.

Immunohistochemical analysis. Sections (5 μm) from formalin-fixed, paraffin-embedded tumor xenografts were prepared. After deparaffinization, endogenous peroxidase activity was blocked. Antibodies were applied after blocking with normal goat serum. Sections were incubated with the anti-rabbit secondary antibody (Santa Cruz Biotechnology) and a streptavidin-HRP followed by exposure to the diaminobenzidine tetrahydrochloride substrate (Dako, Glostrup, Denmark). The sections were counterstained in Mayer's hematoxylin and mounted. Immunostaining signals were scored by two independent observers. Semiquantitative scores were given as the score of the percentage of positive cells plus the score of the staining intensity. The scoring criteria of the percentage of positive cells were as follows: score 0, 0–5% positive cancer cells; score 1, 6–25%; score 2, 26–50%; score 3, 51–75%; and score 4, 76–100% positive. The intensity score was given as follows: score 0, no staining; score 1, weak/equivocal; score 2, moderate; and score 3, strong staining. The final scores were from 0 to 7 and 4 or more was considered positive.

Quantitative DNA methylation analysis of insulin-like growth factor binding protein-3 by real-time PCR (MethyLight assay). Sodium bisulfite treatment of genomic DNA and MethyLight assay were performed as described previously.[21,38] Primer sequences were 5′-GTTTCGGGCGTGAGTACGA-3′ and 5′-GAATCGACGCAAACACGACTAC-3′ for IGFBP-3 and 5′-TGGTGATGGAGGAGGTTTAGTAAGT-3′ and 5′-AACCAATAAAACCTACTCCTCCCTTAA-3′ for β-actin. Probe sequences were 6FAM-5′-TCGGTTGTTTAGGGCGAAGTACGGG-3′-BHQ1 for IGFBP-3 and 6FAM-5′-CCAACACACAATAACAAACACA-3′-BHQ-1 for β-actin.

A percentage of methylated reference (i.e. degree of methylation) cutoff value of 4 was based on previously validated data.[38]

Western blotting. Cells were cultured in serum-free medium for 24 h then stimulated with 20 ng/mL IGF-I or 10 nM insulin. Cell lysates were prepared as described previously.[34] Equal aliquots of lysates (100 μg) were separated by 4–20% SDS-PAGE and immunoblotted onto polyvinylidene Hybond-P membrane (Amersham, Arlington Heights, IL, USA). Analysis was performed using the indicated antibodies, and bands were visualized by ECL (Amersham).

***In vitro* cell growth.** Four thousand cells were seeded into a 96-well plate and each was treated with several concentrations of BMS-536924. Cell growth was measured using WST-1 reagent (Roche, Basel, Switzerland), as described previously.[37]

Colony forming activity. Cells (3×10^3/plate) were seeded onto 60 mm culture plates and incubated for 24 h. The cells were then treated with BMS-536924 and were incubated for 14 days. After air-drying, cells were fixed with methanol and stained with Giemsa solution. Colonies containing 50 cells or more were counted.

Assessment for apoptosis. Caspase-3 colorimetric protease assay was performed following the manufacturer's protocol (MBL, Nagoya, Japan). In brief, the caspase-3 activity of lysates (100 μg) was measured by colorimetric reaction at 400 nm. TUNEL assays were performed with an *in situ* apoptosis detection kit (Takara, Kyoto, Japan) following the manufacturer's protocol.

***In vivo* therapeutic efficacy in established tumors.** One $\times 10^6$ TGBC-1TKB were subcutaneously injected into nude mice. After tumors were palpable (24 days after inoculation), animals were treated orally once daily for 2 weeks, either with BMS-536924 (70 mg/kg) or control. Mice were killed when tumors reached 2 cm in size or they developed clinically evident symptoms. Tumor diameters were serially measured with calipers and tumor volume was calculated using the formula: tumor volume (mm^3) = (width^2 × length)/2.

After TGBC-1TKB tumors became palpable, adenovirus-IGF-IR/dn or adenovirus-lacZ were injected intratumorally for five successive days. Mice were killed on the 47th day.

Statistical analysis. The association between immunohistochemical expression and clinicopathological characteristics were assessed using the Mann–Whitney's *U*-test and Fisher's exact test. The results are presented as means ± SE for each sample. The statistical significance of differences was determined by Student's two tailed *t*-test in two groups and done by one-way ANOVA in multiple groups, and by two-factor factorial ANOVA. *P*-values of <0.05 were considered to indicate statistical significance.

Results

Overexpression of insulin-like growth factor-axis in biliary tract carcinomas tissues. Figure 1 shows representative results of immunohistochemistry for IGF-I, IGF-II, IGF-IR, matrilysin and p53 in BTC. IGF-I-positivity was 60% in total, 57% in GBC, 60% in BDC and 65% in CAV. IGF-I-positivity was significantly correlated with tumor size (Table 1). IGF-II-positivity was 50% in total, 47% in GBC, 53% in BDC and 50% in CAV. IGF-II-positivity was significantly correlated with tumor size, advanced T-stage in GBC, and advanced tumor stage in both BDC and CAV. IGF-IR-positivity was 69% in total, 63% in GBC, 77% in BDC and 65% in CAV. IGF-IR-positivity was significantly correlated with advanced tumor stage in all types and with advanced T-stage in GBC.

Insulin-like growth factor-I-positivity was significantly correlated with IGF-II-positivity in GBC and BDC ($P = 0.028$ and 0.014, respectively). IGF-I-positivity was significantly correlated with IGF-IR-positivity in GBC and tended to be associated with the receptor in BDC ($P = 0.018$ and 0.068, respectively). IGF-II-positivity was significantly correlated with IGF-IR-positivity in GBC, BDC and CAV ($P = 0.021$, 0.025 and 0.029, respectively). IGF-IR-positivity was significantly correlated with matrilysin positivity in GBC, BDC and CAV ($P = 0.010$, 0.016 and 0.007, respectively). IGF-IR-positivity was significantly correlated with p53-positivity in GBC ($P = 0.040$).

The results indicated that the IGF axis might play an important role in tumor development of human BTC and that IGF-IR might interact with p53 in GBC and with matrilysin in BTC.

Hypermethylation of the insulin-like growth factor binding protein-3 promoter in biliary tract carcinomas tissues. Hypermethylation of the IGFBP-3 promoter was observed in 41% of BTC, 43% in GBC, 37% in BDC and 45% in CAV (Table 2). IGFBP-3 methylation was not correlated with clinicopathological characteristics or expression of the IGF-axis. IGFBP-3 hypermethylation was detected more frequently in p53-negative tumors than in p53-positive tumors in GBC, BDC and CAV ($P = 0.016$, 0.021 and 0.025, respectively). Preliminary data indicates that IGFBP-3 hypermethylation is inversely associated with expression of IGFBP-3 mRNA (data not shown). Then, we wanted to assess the possibility of IGF-IR as a molecular target in human BTC.

Blockade of signal transduction. All seven human BTC cell lines expressed IGF-IR detected by real-time PCR (data not shown). To investigate the effect of BMS-536924 on IGF/receptor signaling, we examined three BTC cell lines. First, we evaluated BMS-536924 activity in TGBC-1TKB by Western blotting. One μM BMS-536924 blocked IGF-I-induced phosphorylation

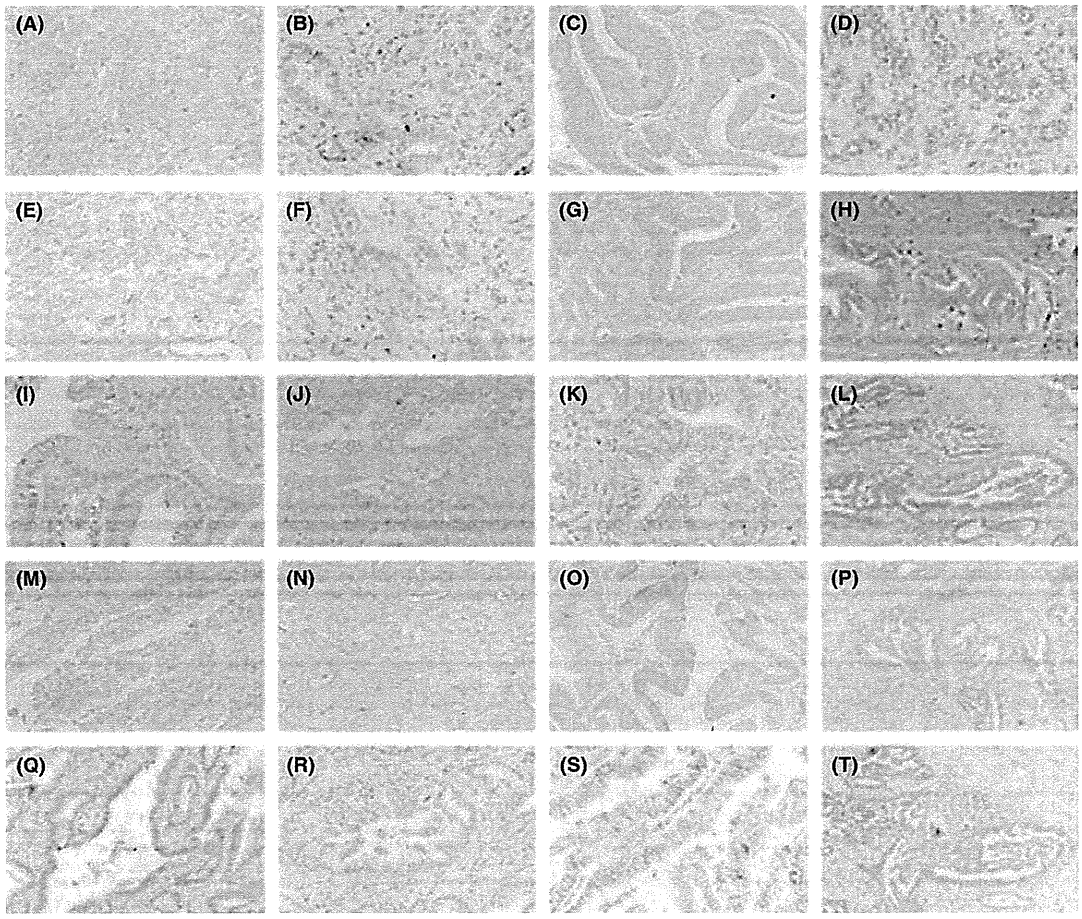

Fig. 1. Immunohistochemical expression of insulin-like growth factor (IGF)-I (A–D), IGF-II (E–H), IGF-I receptor (I–L), matrilysin (M–P) and p53 (Q–T) in gallbladder carcinoma (A, E, I, M, Q), in bile duct carcinomas (B, D, F, H, J, L, N, P, R, T) and in carcinomas of the ampulla of Vater (C, G, K, O, S). Representative pictures show that IGF-I was positively stained in most tumors (A–C) but not all (D). IGF-II was positively immunostained in (E–G) but was negative in (H). IGF-IR was positive in most cancers (I–K) but was negative in some (L). Matrilysin was expressed in most cancers (M–O) but not all (P). Overexpressed p53 was detected in most tumors (Q–S) but not in (T).

doi: 10.1111/j.1349-7006.2011.02138.x

Table 1. Expression of insulin-like growth factor (IGF) axis in biliary tract cancer tissues

	N	IGF-I		P	IGF-II		P	IGF-I receptor		P
		+	−		+	−		+	−	
		17	13		14	16		19	11	
(a) Gallbladder cancer tissues										
Sex										
Male	17	10	7	0.921†	8	9	0.749†	11	6	0.713†
Female	13	7	6		6	7		8	5	
Size										
<25 mm	18	7	11	0.019†	5	13	0.014†	9	9	0.069†
>25 mm	12	10	2		9	3		10	2	
pT										
pT1a	3	1	2	0.260‡	1	2	0.038‡	1	2	0.028‡
pT1b	1	0	1		0	1		0	1	
pT2	8	5	3		2	6		4	4	
pT3	16	9	7		9	7		12	4	
pT4	2	2	0		2	0		2	0	
pN										
pN0	15	7	8	0.231†	5	10	0.136†	7	8	0.064†
pN1	15	10	5		9	6		12	3	
pStage										
pStage I	3	1	2	0.140‡	1	2	0.080‡	1	2	0.001‡
pStage II	5	2	3		1	4		1	4	
pStage IIIA	7	4	3		3	4		3	4	
pStage IIIB	13	8	5		7	6		12	1	
pStage IVA	2	2	0		2	0		2	0	
Matrilysin										
−	15	7	8	0.231†	5	10	0.136†	6	9	0.010†
+	15	10	5		9	6		13	2	
p53										
−	17	9	8	0.461†	6	11	0.145†	8	9	0.040†
+	13	8	5		8	5		11	2	
IGF-I										
−	13				3	10	0.028†	5	8	0.018†
+	17				11	6		14	3	
IGF-II										
−	16							7	9	0.021†
+	14							12	2	

	N	IGF-I		P	IGF-II		P	IGF-I receptor		P
		+	−		+	−		+	−	
		18	12		16	14		23	7	
(b) Extrahepatic bile duct cancer tissues										
Sex										
Male	23	14	9	0.734†	12	11	0.581†	18	5	0.814†
Female	7	4	3		4	3		5	2	
Size										
<25 mm	11	3	8	0.008†	2	9	0.005†	7	4	0.200†
>25 mm	19	15	4		14	5		16	3	
pT										
pT1	8	3	5	0.224‡	2	6	0.059‡	5	3	0.100‡
pT2	5	4	1		3	2		3	2	
pT3	15	9	6		9	6		13	2	
pT4	2	2	0		2	0		2	0	
pN										
pN0	16	8	8	0.206†	6	10	0.067†	10	6	0.061†
pN1	14	10	4		10	4		13	1	
pStage										
pStage I	6	2	4	0.115‡	2	4	0.032‡	2	4	0.006‡
pStage II	16	10	6		7	9		13	3	
pStage III	6	4	2		5	1		6	0	
pStage IV	2	2	0		2	0		2	0	

Table 1. (continued)

	N	IGF-I +	IGF-I −	*P*	IGF-II +	IGF-II −	*P*	IGF-I receptor +	IGF-I receptor −	*P*
		18	12		16	14		23	7	
Matrilysin										
−	6	4	2	0.545†	2	4	0.261†	2	4	0.016†
+	24	14	10		14	10		21	3	
p53										
−	16	10	6	0.940†	7	9	0.225†	11	5	0.256†
+	14	8	6		9	5		12	2	
IGF-I										
−	12				3	9	0.014†	7	5	0.068†
+	18				13	5		16	2	
IGF-II										
−	14							8	6	0.025†
+	16							15	1	

	N	IGF-I +	IGF-I −	*P*	IGF-II +	IGF-II −	*P*	IGF-I receptor +	IGF-I receptor −	*P*
		13	7		10	10		13	7	
(c) Carcinoma tissues of the ampulla of Vater										
Sex										
Male	10	7	3	0.500†	6	4	0.328†	7	3	0.500†
Female	10	6	4		4	6		6	4	
Size										
<25 mm	13	6	7	0.022†	4	9	0.029†	7	6	0.177†
>25 mm	7	7	0		6	1		6	1	
pT										
pT1	5	2	3	0.167‡	1	4	0.093‡	1	4	0.167‡
pT2	6	4	2		3	3		3	3	
pT3	8	6	2		5	3		6	2	
pT4	1	1	0		1	0		1	0	
pN										
pN0	10	6	4	0.500†	4	6	0.328†	5	5	0.175†
pN1	10	7	3		6	4		8	2	
pStage										
pStage IA	3	1	2	0.137‡	1	2	0.049‡	0	3	0.002‡
pStage IB	4	2	2		1	3		1	3	
pStage IIA	4	3	1		1	3		2	2	
pStage IIB	8	6	2		6	2		8	0	
pStage IV	1	1	0		1	0		1	0	
Matrilysin										
−	6	4	2	0.664†	2	4	0.314†	1	5	0.007†
+	14	9	5		8	6		12	2	
p53										
−	12	8	4	0.608†	5	7	0.325†	7	5	0.392†
+	8	5	3		5	3		6	2	
IGF–I										
−	7				2	5	0.175†	3	4	0.151†
+	13				8	5		10	3	
IGF–II										
−	10							4	6	0.029†
+	10							9	1	

†Chi-square. ‡Mann–Whitney's *U*-test. N, number.

of IGF-IR completely (Fig. 2A). This TKI blocked both basal phosphorylation of Akt-1 and ERK and that induced by IGF-I, in a dose-dependent manner. Similarly, in both 2TKB and 14TKB cells, BMS-536924 reduced ligand-induced IGF-IR autophosphorylation and phosphorylation of Akt-1 and ERK with dose dependency.

In both 1TKB and 2TKB (Fig. 2B), 1 μM BMS-536924 also reduced the insulin-induced phosphorylation of InsR and its downstream signal activity with dose dependency. Thus, BMS-536924 effectively interrupted both IGF-I and insulin induced signals in BTC.

Reduction of cell growth *in vitro*. BMS-536924 reduced the growth on plastic of all BTC cells in a dose-dependent manner, as analyzed by the WST-1 assay (Fig. 3A). Moreover, BMS-536924 dramatically reduced the *in vitro* tumorigenicity of all cells dose dependently as assessed by colony formation assay (Fig. 3B). These results indicate that BMS-536924 effectively blocks the carcinogenicity and proliferation of BTC.

doi: 10.1111/j.1349-7006.2011.02138.x